Organic geochemical, palynofacies, and petrographic analyses examining the hydrocarbon potential of the Cretaceous (Albian) Kharita Formation in the Matruh Basin, northwestern Egypt

Amr S. Deaf [ID, 1, 4], Sameh S. Tahoun[2], Thomas Gentzis[3], Humberto Carvajal-Ortiz[3], Ian C. Harding[4], John E. A. Marshall[4], Seare Ocubalidet[3]

[1] Geology Department, Faculty of Science, Assiut University, Assiut, 71516, Egypt
[2] Geology Department, Faculty of Science, Cairo University, Giza, 12613, Egypt
[3] Core Laboratories, 6316 Windfern Road, Houston, TX 77040, USA
[4] School of Ocean and Earth Science, National Oceanography Centre, University of Southampton, European Way, Southampton, SO14 3ZH, UK

Corresponding author e-mail: amr.daif@science.au.edu.eg, asdeaf75@yahoo.com
Amr S. Deaf ORCID ID: http://orcid.org/0000-0002-5073-7911

Abstract

A recent study of selected samples from the Cretaceous (Albian) Kharita Formation of Egypt revealed very good to excellent source rock (SR) potential for six intraformational, organic-rich intervals. This work investigates the SR potential of the entire Kharita Formation across the Matruh Basin, using samples from two wells: the Abu Tunis 1X well from the central part of the basin, and the Siqeifa 1X well drilled on the eastern margin of the basin. More strongly reducing conditions were developed in the centre of the basin, and resulted in the deposition of more organic-rich shales by comparison to the less reducing conditions that prevailed on the eastern basin margin, where the shales contain less organic matter. Deltaic intraformational shales and carbonates in the Kharita Formation of Abu Tunis 1X constitute a significant 120 m net of the potential SR. The lower Kharita Formation contains 34 m net shale SR of good to very good/excellent organic richness, yielding values of 1.14–11.59 wt % total organic carbon (TOC). The organic matter has low Hydrogen Index (HI) values (184–389 mg HC/g TOC) and amorphous organic matter (AOM) and relatively high non-opaque phytoclast frequencies indicating mainly gas/oil-prone organofacies (kerogen types II/III). The upper Kharita is more important, containing 86 m net shale/carbonate SR that has fair to good organic richness (0.8–1.8 wt % TOC), and lower HI (126–250 mg HC/g TOC), a dominance of non-opaque phytoclasts, and subordinate AOM frequencies, which together

indicate gas/oil-prone organofacies (kerogen Types III/II). In the Siqeifa 1X well, Kharita deltaic intraformational shales and shaley dolostones comprise 80 m net SR, which has mainly fair to good to less very good organic richness (0.8–2.1 wt % TOC), whilst low HI (93–220 mg HC/g TOC), dominance of non-opaque phytoclasts and subordinate AOM indicate gas-prone organofacies (kerogen Type III). A relative upward increase in deposition of lignite and coaly carbonaceous material supports a gas-prone organofacies. Whilst thermal maturity indices only point to immature to early mature (pre- to early oil-window) SRs in both the Abu Tunis 1X and Siqeifa 1X wells, hydrocarbon exploration focussing on this potential source rock may be justified in areas to the southeast of the Matruh Basin, where modelling indicates this unit may have reached the late mature oil- to main gas-generation window.

Keywords: Palynofacies, Organic petrology; Rock-Eval pyrolysis; Organofacies; Hydrocarbon potential; Kharita Formation; Matruh Basin; Egypt

1. Introduction

Lower Cretaceous Albian strata in the northern and southern Mediterranean regions contain intraformational organic-rich deposits which show significant hydrocarbon source rock potential, such as in SE France (Herrle et al., 2003; Bornemann et al., 2005), Italy (Katz et al., 2000), and Tunisia (e.g., Ben Fadhel et al., 2011; Khalifa et al., 2018). However, information on the organic richness and petrography, and hence the hydrocarbon source rock potential of the Albian deposits of the southeastern Mediterranean area, specifically of Egypt, is still fragmentary. The only recent hydrocarbon study was carried out by Gentzis et al. (2019) on the Albian Kharita Formation in the Abu Gharadig Basin in the north Western Desert of Egypt. Within the north Western Desert, the Matruh area is typically regarded as one of the important hydrocarbon producing basins amongst the other costal basins, namely the Shushan, Dahab–Mireir (= Alamein), and Natrun (Fig. 1). The Matruh Basin holds about 23 BBOE of known oil (Shahin, 1992) and about 3 TCF of gas reserves (Metwalli et al., 2018), and the main Mesozoic hydrocarbon source rocks are the Middle Jurassic upper Khatatba, the Lower Cretaceous (Berriasian–

Barremian) Alam El Bueib, and the Upper Cretaceous (middle–upper Cenomanian) “G” Member of the Abu Roash formations (Fig. 2). The hydrocarbon reservoirs are represented by the lower Khatatba, Lower Cretaceous (Aptian) Alamein, (Albian) Kharita, Upper Cretaceous (Cenomanian) Bahariya, and (Turonian) “D” Member of the Abu Roash formations (e.g., Aram et al., 1988; EGPC, 1992; Shalaby et al., 2011; Abrams et al., 2016; Tahoun and Deaf, 2016; Deaf and Tahoun, 2018).

The Kharita Formation of the north Western Desert of Egypt is a classical hydrocarbon reservoir (e.g., Meshref, 1996), deposited in a deltaic setting during a regressive phase (Said, 1990; Deaf, 2009; Mahmoud et al., 2019), where fine to coarse sandstone is the dominant lithology but subordinate shale intercalations also occur (Hantar, 1990). This resulted in the Kharita Formation being largely organic-poor, and having better reservoir quality rather than source rock potential in most of the north Western Desert (EGPC, 1992). Indeed, in the neighbouring coastal Shushan and Sidi Barani basins (Fig. 1), the Kharita Formation has been demonstrated to possess only poor to fair gas source rock potential (avg. 0.83 wt % TOC, avg. HI 44.5 mg HC/g TOC, and Tmax 429–435 °C) in the El Noor well of the Sidi Barani Basin (Aboul Ela et al., 2018). Similarly, to the south of the costal basins, the Kharita Formation in the Abu Gharadig Basin has a very low gas source potential (avg. 0.71 wt % TOC, avg. HI 149 mg HC/g TOC, and Tmax 426–438 °C), and better reservoir properties (Gentzis et al., 2019). These properties are related to the high sandstone volume and very low volumes of (organic-poor) shale (Metwalli and Pigott, 2005; Aboul Ela et al., 2018). However, a quantitative organic petrographic analysis carried out by Deaf (2009) on thirty-nine palynological samples of the Kharita Formation in the Abu Tunis 1X well in the Matruh Basin identified the presence of six organic-rich horizons that contain exceptional abundances of AOM (500,000–700,000, avg. 572,000 particles/gram of dry sediments; Fig. 3). Geochemical evaluation by Tahoun et al. (2017) of these samples has indicated very good to excellent hydrocarbon source potential for these six fine clastic (mainly shales), organic-rich intervals. The total organic carbon content of these Albian samples ranged from 2 to 11.6 wt % with an average of 3.4 wt %, and S_2 values which ranged from 1.1 to 23.5 mg HC/g dry rock (avg. 8 mg HC/g dry rock). The calculated HI (165–318, avg. 228 mg HC/g TOC) and organic petrographic analyses (light microscopic palynofacies and UV fluorescence) indicated a mixture of kerogen Types III and II. Thermal maturation indices indicated immature to early mature (early oil-window) stage of maturity for these sample, with values for Tmax of 416–428 °C (avg. 421 °C), vitrinite reflectance of 0.49–0.58 % Rv, and a thermal alteration index (TAI) of 2 to 2+.

To our knowledge, the current investigation presents the first organic petrographic analysis of the Albian Kharita Formation deposits in Egypt from the Matruh Basin, integrated here with organic geochemical and palynological analyses to evaluate the hydrocarbon potential of this historically neglected formation.

The hydrocarbon potential of source rocks has conventionally been assessed using organic geochemical parameters alone (e.g., Shalaby et al., 2011, 2012; Makky et al., 2014). Other investigations combined reflected white light (RWL) petrography and organic geochemical analyses of the organic matter to study the hydrocarbon potential of source rocks (e.g., Espitalié et al., 1985; Mukhopadhyay et al., 1989; Powell and Boreham, 1994; Shalaby et al., 2012; Hazra et al., 2015). Other studies have emphasised organic facies analysis, based on the RWL examination of the organic matter (Suárez-Ruiz, et al. 2012; Mendonça Filho et al., 2017), while the role of transmitted white light (TWL) petrography has been minor. Here, we propose a practical and productive protocol, based on the integration of organic petrographic (TWL, RWL, and ultraviolet fluorescence = UVF), palynofacies, and geochemical analyses of the organic matter that can be applied to any formation being studied in any basin, worldwide (Fig. 4). This protocol provides visual characterization and quantification of the kerogen constituents via TWL petrography, which is then correlated to kerogen characteristics defined using RWL. Moreover, this method overcomes the limitations of Rock-Eval analysis, such as the problems with identifying kerogen types due to mixing/averaging of reactive and inert kerogen types. RWL analysis does have certain limitations, whereby it cannot provide a detailed visual characterization of the different maceral constituents and cannot infer the botanical precursors of the organic matter in detail (Suárez-Ruiz et al., 2012; Mendonça Filho et al., 2017). The above problem was largely solved by Mendonça Filho (2012) who proposed palynological working groups (WG), a scheme which permits kerogen/maceral types to be correlated between TWL and RWL techniques. This cross correlation was successfully applied in the current study, and provided a good means of calibration between the TWL-based (i.e., spore colouration) and the RWL-based (i.e., vitrinite reflectance/UV fluorescence) thermal maturity analyses. Furthermore, most hydrocarbon exploration studies have identified the environmental settings of the organic facies mainly based on RWL organic petrography and geochemical analyses (e.g., Singh et al., 2017b). In this study, we will present an interpretation of the depositional environments based mainly on integrating palynological and sedimentological data. This approach has been widely used in several palynological studies and provides important information on the source and the environmental parameters that controlled the accumulation and preservation of organic matter (e.g., Tyson, 1996; El-Soughier et al., 2014; Tahoun and Deaf, 2016; Mahmoud et al., 2017; Tahoun et al., 2017; Deaf and Tahoun, 2018; Deaf et al., 2019). Palynological analysis enjoys the merit of being simple and cost effective as it needs no further laboratory preparations, uses the same slide-mounted organic matter used for the thermal maturity analysis (i.e. TAI), and provides rapid but informative interpretations. On the other hand, several hydrocarbon investigations were based mainly on TWL (i.e., palynofacies) and geochemical analyses (e.g., Alaug et al., 2014; Tahoun and Deaf, 2016; Deaf and Tahoun, 2018). Recently, Gentzis et al. (2018) used an approach, similar to the one we propose here, to study the hydrocarbon potential of some Egyptian Upper Jurassic sediments, but without employing the organic facies concept. Thus, the current investigation aims to present a balanced and integrated TWL/RWL organic petrographic, palynofacies, and geochemical identification of the organic facies of the Egyptian Albian Kharita Formation to explore the hydrocarbon potential of this neglected unit at both the basin centre and the eastern margin of the Matruh Basin.

2. Geological setting and stratigraphy

The Matruh Basin is a Late Jurassic–Early Cretaceous graben with a NNE–SSW orientation, and lies approximately between longitudes 26° and 27° 30’ E and latitudes 31° and 31° 17’ N (EGPC, 1992; Meshref, 1996; Guiraud and Bosworth, 1999; Shalaby et al., 2012). It is bounded to the northwest by the Sidi Barani High and to the South by the Ras Qattara High (Fig. 1). The Matruh basin was originally formed as one large continental basin made of the Matruh-Shushan Basin during the Permo-Triassic (Meshref and Hammouda 1990; Abdel Halim and Moussad, 1992). It developed later as a rift basin during the late Cimmerian Orogeny as a result of the separation of the northern African plate from the European plate (Meshref, 1996). In most of the basin area, the sedimentary sequence ranges in age from the Cambrian to the Miocene (Fig. 2), while in other parts of the basin the Cambrian to Middle Jurassic is represented by basement (Aram et al., 1988).

Sedimentation in the Matruh Basin was controlled largely by tectonics, where four major sedimentary cycles are separated by regional unconformities (Sultan and Halim, 1988). The first cycle was developed during the Early-Mid Jurassic, where the fluvio–lacustrine sediments of the Ras Qattara and Yakout formations and the deltaic and shallow marine sediments of the Khatatba and Masajid formations were deposited (Fig. 2). The Lower–Upper (Albian–middle Cenomanian) Cretaceous fluvio–deltaic to shallow marine sediments of the Alam El Bueib, Alamein, Dahab, Kharita, and Bahariya formations represent the second cycle. The uppermost (upper Cenomanian–Campanian) Cretaceous open marine shales of the Abu Roash and carbonates of the Khoman formations represent the third cycle, whilst the fourth cycle consists of the upper Paleogene–lower Neogene (Eocene–Miocene) open marine shale and carbonates of the Apollonia, Dabaa, Moghra, and Marmarica formations.

Lithostratigraphically, the Kharita Formation was introduced by Norton (1967) as a member of the Burg El Arab Formation, Ghorab et al. (1971) later reclassifying it as a formation. According to Said (1990) the Kharita is a clastic unit of Albian age, comprised of fine- to coarse-grained sandstones with subordinate shale and carbonate horizons (Hantar, 1990; Kerdany and Cherif, 1990), and its type locality located in the interval between 2501 to 2890 m in the Kharita-1 well in the Abu Dahab-Mireir Basin (Fig. 1). In the north Western Desert area, including the Matruh Basin, the Kharita Formation conformably overlies upper Aptian shales and fine sandstones of the Dahab Formation and conformably underlies the middle Cenomanian clastic and carbonate units of the Bahariya Formation. The Kharita has been interpreted as being deposited in fluviatile to shallow marine settings during a major marine regressive episode (Hantar, 1990; Said, 1990). Palynological investigations (e.g., El-Soughier et al., 2014; Aboul Ela et al., 2018) have also suggested deltaic to marginal marine environments for the Kharita Formation in several areas of the north Western Desert of Egypt (e.g., Abu Dahab–Mireir and Abu Gharadig). In the Matruh

Basin, the Kharita Formation was deposited during a pronounced regressive phase in marginal marine settings in the area of the Siqeifa 1X well (Mahmoud and Deaf, 2007) and in deltaic to shallow marine settings in the area of the Abu Tunis 1X well (Deaf, 2009; Deaf et al., 2019).

In the Abu Tunis 1X well, the Kharita Formation is composed of medium- to fine-grained argillaceous sandstones with a carbonate and/or silicic matrix and contain traces of pyrite, bulk coaly carbonaceous material and infrequent traces of anhydrite. These argillaceous sands are intercalated with thin light grey to green fissile shales that contain traces of macroscopic black coaly carbonaceous material. The Kharita Formation in the Abu Tunis 1X attains a thickness of 1700 ft (518.2 m). In the Siqeifa 1X well, the Kharita Formation is 1550 ft (472.4 m) thick and is mainly composed of fine- to coarse-grained argillaceous sandstones that are intercalated with thin, light to medium grey fissile to massive shale horizons. The sandstones possess dolomitic cement and contain traces of low-rank coal (lignite) and/or bulk coaly carbonaceous material, in addition to frequent traces of pyrite and glauconite. Shale intercalations contain traces of pyrite and glauconite and infrequent traces of lignite.

Mahmoud and Deaf (2007) and Deaf et al. (2014) studied the palynostratigraphy of the Albian Kharita Formation in the Siqeifa 1X and Abu Tunis 1X wells respectively. In the Abu Tunis 1X well, the drilling company WEPCO (1968) did not identify the lower part of the unit being studied here with any particular formation, and described its upper part as simply “Cenomanian Clastics”. However, based on palynological and lithological data, Deaf et al. (2014) identified this section of the Abu Tunis 1X stratigraphy as the Kharita Formation, and proposed an Albian age. In the Siqeifa 1X well, WEPCO (1970) did not identify the lower part of the clastic sequence we study here, and identified the upper part of this sedimentary sequence as “Cenomanian Carbonates”. Mahmoud and Deaf (2007) suggested an Albian age for this clastic unit, and combining this age with the dominant sandstone lithology, we believe that the clastic unit in the Siqeifa 1X well also represents the Kharita Formation, which is known to have an Albian age across the north Western Desert of Egypt (Said, 1990).

3. Materials and methods

3.1. Open-system programmed pyrolysis (Rock-Eval pyrolysis)

Twenty–eight samples from the Abu Tunis 1X well and twenty–five samples from the Siqeifa well were analyzed by open-system programmed pyrolysis analysis (Tables 1 and 2). The instrument utilized was a Rock-Eval® 6 Turbo unit (RE6) made by Vinci Technologies, France. The pyrolysis method used was the Basic/Bulk-Rock method (IFP Rock-Eval methods®) typically utilized for source rock evaluation. Briefly, 60 mg of pulverized sample were weighed and placed inside a stainless-steel crucible. The sample was first decomposed in the pyrolysis oven under a nitrogen atmosphere to obtain the weight % of pyrolyzable carbon (PC) and pyrolyzable mineral carbon. Hydrocarbons and both CO and CO_2 were detected simultaneously by a flame ionization detector (FID for hydrocarbons) and infrared cell (IR for CO_2 and CO). Subsequently, each sample was combusted in the oxidation oven to obtain the weight % of residual carbon (RC) and oxidized mineral carbon (oxiMinC). The temperature program for the pyrolysis cycle was 300 °C isothermal for 3 min followed by a 25 °C/min ramping from 300 °C to 650 °C. The oxidation program was 300 °C isothermal for 60 s followed by a 25 °C/min ramping from 300 °C to 850 °C, held isothermal for 5 min at 850 °C. For more details, the reader is referred to Behar et al. (2001).

3.2. Transmitted light microscopy: palynology and palynofacies analysis

The standard HCl/HF maceration techniques of Phipps and Playford (1984) and Green (2001) were followed to extract the palynological matter (PM) as it is referred to by the palynological community for the transmitted white light (TWL) petrographic and palynofacies analyses (e.g., Batten and Stead, 2005; Traverse, 2007). A sum total of fifty–nine ditch-cutting rock samples (34 from Abu Tunis 1X and 25 from Siqeifa 1X) were collected. Three grams of each sample from the Abu Tunis 1X well were processed, and spiked with one tablet of modern *Lycopodium* spores (12,542 grains/tablet with V ± 3.3 %) by Deaf (2009) at the School of Ocean and Earth Science, National Oceanography Centre, University of Southampton, UK. Samples were sieved through a 15 µm mesh and organic residue from each sample was strewn onto two cover slips, dried and later mounted on microscope slides using Elvacite 2044. Ten grams of each sample from the Siqeifa 1X well were processed by Deaf (2002) using the standard HCl/HF maceration at the Geology Department, Faculty of Science, Assiut University, Egypt. The organic residues stored at the Geological Museum of the Geology Department (Faculty of Science, Assiut University) were resuspended with distilled water and few drops of each residue were mounted onto each of two microscope slides using Canada Balsam.

Palynofacies analysis was carried out on the PM residues recovered from 34 samples of Abu Tunis 1X and from 16 out of 25 samples available after the Rock-Eval and vitrinite reflectance analyses of Siqeifa 1X using the TWL Olympus (BX41) microscope at the Geology Department, Faculty of Science, Assiut University. For qualitative palynofacies analyses, the identification and classification of the PM (kerogen) constituents were made following Tyson (1995) and the recently updated classification presented by Mendonça Filho et al. (2012) and Mendonça Filho and Gonçalves (2017). Quantitatively, separate counts of 500 particles of the kerogen constituents ('palynodebris' or macerals), i.e., palynomorphs, translucent and opaque phytoclasts and AOM (Tables 5 and 7), and of 300 palynomorphs (Tables 3 and 4) were carried out for each sample, following Tyson (1995, p. 439) and Deaf and Tahoun (2018). The separate palynomorph count was undertaken to counter the dilution effect of other "kerogen" constituents to the palynomorphs (Tyson, 1995) and to obtain a statistically meaningful representation of different organic matter entities (e.g., Tyson, 1995). For the interpretation of depositional environments of the Siqeifa 1X well rocks, eight palynological categories based on two subsets of the organic matter were used, namely the total palynomorphs and the total PM (see tables 4 and 8; e.g., Tyson, 1995; Mahmoud et al., 2017; Deaf and Tahoun, 2018). Thus, the percentage frequencies of the terrestrial and marine palynomorphs are derived from total palynomorphs, while those of the kerogen constituents are derived from the total kerogen. Furthermore, the percentage frequency data derived from the raw count of 300 palynomorphs was normalized to 100% (Suárez-Ruiz, et al., 2012) and plotted in the Spores–Microplankton–Pollen (SMP) ternary diagram of Federova (1977) and Duringer and Doubinger (1985) to interpret the depositional environment (tables 3 and 4). Similarly, the normalized percentage frequency data derived from the total (kerogen) count of 500 particles (Tables 5 and 7) was plotted on the Liptinite–Vitrinite–Inertinite (LVI) ternary diagram of Dow (1982) and Tyson (1995) to identify hydrocarbon generation potential, and on the AOM–

Phytoclasts–Palynomorphs (APP) ternary plot of Tyson (1995) to identify the depositional environment and redox conditions (see Table 6; Tyson, 1995). It is important to note that the maceral analysis made for the LVI plot was performed on the PM (kerogen) concentrates through a series of non-overlapping traverses across the strew slides using the TWL microscope. The 500 particles of the three main groups of the PM (palynomorphs, phytoclasts, and AOM) were counted closest to the centre of the field of view according to Tyson (1995) and Mendonça Filho (2012). The counted particles were then related to their macerals and maceral groups as identified under RWL microscopy according to the International Committee for Coal and Organic Petrology (ICCP) palynofacies working group (see Mendonça Filho et al., 2012). Under the latter scheme, opaque phytoclasts are not assigned a specific maceral type but have been allocated to the maceral group inertinite; non-opaque, biostructured phytoclasts were identified as belonging to either the maceral telinite or to the maceral group vitrinite. Other non-opaque, membranous and cuticular phytoclasts have been allocated to the maceral cutinite and the maceral group liptinite. Sporomorphs and dinoflagellate cysts have been identified as the macerals sporinite and lamalginite respectively, and to the maceral group liptinite. Finally, AOM and highly degraded macrophyte tissues are equated with the maceral bituminite and the maceral group liptinite.

The palynological marine index (PMI) of Helenes and Somosa (1999) was calculated according to the following formula:

$PMI = Rm\ (1+/Rt)*\ 100$

where,

Rm = the counted number of marine palynomorphs (dinoflagellate cysts and microforaminiferal test linings) per sample

Rt = the counted number of terrestrial palynomorphs (spores, pollen grains, and freshwater algae) per sample.

According to Helenes and Somosa (1999), a zero value of the PMI indicates a terrestrial environment without any form of marine signal. Low PMI values (~ 50–100) indicate marginal marine environments with brackish water conditions, whilst a PMI > 200 indicates deeper marine/offshore environments. It should be borne in mind that Helenes and Somosa (1999) used this formula to help interpret depositional environments of samples showing low to moderate palynomorph recovery, where they used total counts of 100 grains, so that counts of 300 grains will be more statistically meaningful (see Traverse, 1988, p. 490; Tyson, 1995, p. 433).

The quantitative absolute abundance analysis (grains/gram) of the Abu Tunis 1X PM constituents was completed by Deaf (2009) to counter the data closure effect of the relative abundance (percentage) analyses, and to identify any differences between the two datasets. However, it was found that the vertical percentage distribution of single organic matter entities is consistent with that of the absolute abundance data trends, especially for samples are dominated by AOM and phytoclasts, although certain palynomorphs show minor differences in trends (see Fig. 3 and Table 5).

The visual identification of spore colour in terms of the thermal alteration index (TAI) of Pearson (1990) was undertaken on selected smooth spore grains from the total 300 palynomorphs count to identify the degree of thermal maturation of the organic matter.

3.3. Reflected light microscopy: vitrinite reflectance (Rv) and fluorescence

The detailed sample preparation and analysis procedures employed here are described in the ASTM D7708 standard test method (2014) and also by Hackley et al. (2015). Briefly, whole-rock (WR) cuttings samples were crushed to -20 mesh size (0.85 mm) particles. Ground particles were placed in specially designed plastic moulds (3.2 cm in diameter), mixed with Epo-Thin epoxy resin and hardener (ratio of 2:1) and left to cure overnight. The resulting pellets were ground and polished using a Buehler EcoMet/AutoMet 250 automated polisher using a combination of 320 μm and 600 μm cloths and polished using a combination of two stages of a slurry of alumina powder (0.3 and 0.05 μm) and water. Vitrinite random reflectance (%Rv) and fluorescence analyses were performed on the dispersed organic matter (DOM) using a Carl Zeiss A2m Axio Imager RWL microscope equipped with white (halogen) light source (12V/100W). A 50x oil immersion objective (noil = 1.514 at 23^{o}C) was used for a combined magnification of 500x. Qualitative UV analysis was performed using the same microscope with high-pressure Hg lamp (HBO 100W) in the fluorescence mode (FM). The excitation filter had a wavelength of 465 nm and the combined dichroic mirror and barrier filter a wavelength of 515 nm. For additional information concerning sample preparation protocol, see ASTM D 2797/D2979M-09 (2007). The description and classification of the different kerogen constituents under RWL and FM were made following the standard terminologies presented by the ICCP (1998, 2001) and Pickel et al. (2017).

4. Results and discussion

4.1. Source rock potential

The combined TOC (wt %) and S_2 (mg of HC per gram of rock) data were used together in order to determine the source rock potential of the Kharita Formation, as suggested by Peters and Cassa (1994) and Dembicki (2009), for the reason that elemental analysis of TOC takes into account the "non-reactive organic carbon" (i.e., inertinite material), which is not capable of generating hydrocarbons (Peters and Cassa, 1994; Hart and Steen, 2015). The S_2 parameter measures the remaining (i.e., present-day) hydrocarbon generative potential, from the pyrolytic degradation of the kerogen and heavy hydrocarbons. Thus, the S_2 parameter is regarded as a more informative indicator of the source rock potential when compared to the TOC parameter (Peters and Cassa, 1994; Dembicki, 2009, 2016). In the Abu Tunis 1X well, the deltaic deposits of the lower Kharita Formation from 7300–6450 ft (2225–1966 m) are characterized mainly by organic-rich intraformational shale intervals, and such lithologies have been identified as potential source rocks in previous studies, such as Shalaby et al. (2011) and Abrams et al. (2016), which comprise a net shale content of about 13.1 % (WEPCO, 1968). The lower Kharita Formation contains several shale intervals ranging in thickness from 1.5 to 9.8 m. These shale intervals show notable intraformational variations in organic richness, where they show good to very good/excellent hydrocarbon source potential (1.14–11.59, avg. 4.19 TOC wt %; S_2: 2.72–23.53, avg. 10.41 mg HC/g; Figs. 5a, b, Table 1; see Baskin, 1997). One intraformational sandstone sample was analysed from 6850 ft/2087.9 m and yielded 0.52 wt % TOC, and thus it does not possess source rock characteristics, but would be better regarded as a reservoir unit. The abovementioned geochemical and lithological data indicate that the lower Kharita Formation contains about 34 m net source rock.

The upper Kharita Formation (6449.9–5600 ft/1965.9–1707 m) is composed mainly of less organic-rich argillaceous and/or carbonaceous sandstones and intercalations of limestone, dolostone, and fewer shales. Shale intervals comprise 9.8 % (25.3 m) of the upper Kharita and range in thickness from 3.7 to 12.2 m, while limestone and dolostone intervals comprise 23.4 % (60.6 m) and range in thickness from 6.7 to 39.6 m (WEPCO, 1968). Shale and carbonate intervals show little in the way of intraformational variation in organic richness and has fair to good hydrocarbon source potential (0.82–1.78, avg. 1.10 TOC wt %; S_2: 1.07–4.02, avg. 2.0 mg HC/g). Sandy intervals (three samples analysed from 6100 ft/1859.3 m, 6050 ft/1844 m and 5800 ft/1767.8 m) are organic-lean (0.53–0.78, avg. 0.64 TOC wt %) and are considered reservoirs. Based on the geochemical and lithological data advanced above, it is shown that shale and carbonate intervals comprise a net source rock interval of about 33.2 % (86 m) of the upper Kharita Formation. The cross-pot of S_2 against TOC indicates that the Kharita Formation has a fair to excellent source rock potential (Fig. 5c).

In the eastern margin of the Matruh Basin in the Siqeifa 1X well, the Kharita Formation shows a fair to good source rock potential (Figs. 5a–c, Table 2). The lower Kharita Formation from 7400–7000 ft (2255.5–2133.6 m) contains a higher intraformational shale content at 23.8 %, which comprises 29 m net shale content of the lower Kharita interval (121.9 m) and ranges in thickness from 3.4 to 9.1 m. The lower Kharita Formation also contains a shaley dolostone unit, which represents about 7 % (8.5 m) net fine deposits of that part of the formation according to WEPCO (1970). Shale and shaley dolostone intervals show little intraformational variation in organic richness and have fair to good source rock potential (0.81–1.14, avg. 1.0 TOC wt %; S_2: 1.06–1.69, avg. 1.26 mg HC/g). The argillaceous and carbonaceous sandstones (three samples analysed from 7250 ft/2209.8m, 7200 ft/2194.6 m and 6850 ft/2087.9 m) are less organic-rich (0.55–0.73, avg. 0.66 TOC wt %), and, thus are considered as reservoir intervals. The combined geochemical and lithological data indicates that the lower Kharita interval contains a total of about 30.7 % (37.5 m) net source rock.

The upper Kharita Formation (6999.9–5850 ft/2133.5–1783.1 m) shows a slight upward increase in organic richness (Figs. 5a, b, Table 2), which is related to the deposition of more frequent strings of lignitic and coaly carbonaceous material (Fig. 9) as was recorded by WEPCO (1970). Shale intervals are more frequent but comprise a net shale content of about 12.1 % (42.4 m) of the upper Kharita interval (350.5 m) and range in thickness from 2.7 to 6.7 m (WEPCO, 1970). Shale and coaly shale intervals show fair to good gas-prone source rock potential (0.82–2.14, avg. 1.33 TOC wt %; S_2: 0.88–4.70, avg. 2.10 mg HC/g). Argillaceous sandstones and dolostones (three samples analysed from 6800 ft/2073 m, 6700 ft/2042.2 m and 6000 ft/1829 m) show only poor to fair organic richness (0.35–0.67, avg. 0.49 TOC wt %). Thus, the upper Kharita Formation is shown to contain 42.4 m (or 12.1%) net source rock.

As demonstrated here, the intra-formational variations in organic richness require the application of integrated lithofacies, palynofacies, and petrographic (TWL and RWL) analyses to understand the environmental settings and the controlling factors acting on the organic richness, and to overcome the averaging problem of the TOC and S_2 organic richness parameters.

4.2. Environmental settings and their impact on kerogen preservation and quality

Deaf (2009) and Deaf et al. (2019) interpreted the clastic deposits of the Kharita Formation in the Abu Tunis 1X well as being deposited during a regressive phase of sedimentation in deltaic to shallow marine environments. A plot of the main terrestrial and marine palynomorphs using the SMP ternary diagram of Tyson (1995) also supports a deltaic to shallow marine depositional setting for the Kharita deposits in the Abu Tunis 1X well (Fig. 6a). The proximal setting and the development of regional humid climatic conditions during the Albian–Cenomanian (Deaf et al., 2019) likely promoted flourishing of continental vegetation, associated with high run-off and delivery of the large influxes of terrestrial organic matter into the deltaic environment in which the Kharita Formation was deposited (Lamberson et al., 1991; Tyson, 1995). A plot of the main PM constituents in the APP ternary diagram of Tyson (1995) indicates prevalence of reducing (suboxic–anoxic) conditions during deposition of the Kharita Formation in the vicinity of Abu Tunis 1X (Figs. 7a and 8). Thus, favourable reducing conditions resulted in the deposition of organic-rich clastics within the Kharita Formation at Abu Tunis, in marked contrast to the widely distributed organic-poor clastics of the Kharita Formation across most of the rest of the north Western Desert (Meshref, 1996; Metwalli and Pigott, 2005). The occurrence of lower quantities of terrestrial organic matter in the marginal and shallow marine deposits of the underlying Alam El Bueib and Alamein formations (Fig. 3), when regional climate was relatively drier in comparison to that of the Albian–Cenomanian (Deaf, 2009; Deaf et al., 2019), supports our contention that humid climatic conditions had an effect on the organic richness in the Kharita of Abu Tunis 1X. Adding to this idea, the depositional cyclicity of the deltaic environment, as reflected in the sedimentary facies (sandstone and shale alternations) and the self-potential (SP) log of the Kharita Formation (Deaf et al., 2019, fig. 6) also affected kerogen quality, where kerogen Type III is alternates with and/or is mixed with Type II (Fig. 8). The coarse-grained sandstones are dominated by vitrinite (kerogen Type III), whilst the fine-grained siltstones and shales are dominated by the liptinite (kerogen Type II). This is explained by the fact that high abundances of brown wood (Type II) tend to concentrate in coarse siltstones and very fine sandstones of the proximal depositional settings that are close to land vegetation (e.g., Habib, 1983; Firth, 1993; Tyson, 1995), whereas the finer particulate organic matter (i.e., AOM) and miospores, typically smaller in size by comparison to the brown wood particles found here, tend to concentrate in the fine sandstone, siltstone, and shale lithologies (Batten, 1974; Bujak et al., 1977; Tyson, 1995). Furthermore, those shale intervals within the Kharita Formation of the Abu Tunis 1X well (Fig. 5a, Table 1) that are exceptionally organic-rich (from 4.41-11.60 wt % TOC) may be related to the Albian Oceanic Anoxic Event OAE 1b (Tahoun et al., 2017). On the eastern margin of Matruh Basin, the Kharita Formation in the Siqeifa 1X well shows lower organic richness and quality (Table 2). This is related to the more marginal marine depositional setting of the formation (Mahmoud and Deaf, 2007). Detailed analysis of the allochthonous (sporomorphs, non-opaque and opaque phytoclasts) and autochthonous (dinoflagellate cysts and microforaminiferal test linings = MFTLs) organic matter again suggests deposition in a deltaic environment. This is based on the very high abundance of terrestrially derived organic matter (miospores and phytoclasts) and the very low abundance of dinoflagellate cysts (Fig. 9). The rare occurrence and low species diversity (a total of 10 species) of the dinoflagellate cysts, which are mainly dominated by the restricted, low salinity genera *Subtilisphaera, Odontochitina,* and *Cribroperidinium* (Mahmoud and Deaf, 2007, p. 216, fig. 4) also suggest deposition in proximal marginal marine (brackish–coastal) conditions (e.g., Mutterlose and Harding, 1987; Tahoun and Deaf, 2016; Deaf and Tahoun, 2018; Deaf et al., 2019). The high influxes of spores at the expense of spherical pollen grains (mainly *Arucariacites*) also suggests sedimentation in nearshore settings during a regressive episode, as high frequencies of spores are known to characterize delta-top and delta-front sand, silt and shale deposits (e.g., Degens and Mopper, 1976; Batten, 1982; Tyson, 1995). Similarly, the very high abundances of non-opaque phytoclasts indicate deposition in proximal marginal environments that were close to the fluvio-deltaic systems (e.g., Pocklington and Leonard, 1979; Tyson, 1995). The dominance of sandstones in which the few shale horizons are intercalated and high occurrences of non-opaque and opaque phytoclasts suggests deposition in proximal, shallow water marginal settings under relatively high-energy conditions, probably in the partly submerged bioturbated delta-front setting, an environment characterized by strong influxes of non-opaque and opaque phytoclasts (Tyson, 1995; Deaf et al., 2019). A deltaic setting is also indicated by the SMP ternary plot of the Siqeifa 1X well data (Fig. 6b). This type of setting is characterized by a highly fluctuating water table and strong water circulation (Boggs, 2006), where short-lived reducing (dysoxic–anoxic) conditions, as indicated by the APP ternary plot (Fig. 7b), and reflected by the frequent traces of pyrite, resulted in preservation of low concentrations of AOM mainly in the laminated Kharita shales (see Tyson, 1995). The lignite and bulk coaly carbonaceous material and pyrite are mainly associated with the sandstone units (Fig. 9), interpreted by Singh et al. (2017a) as indicating brackish water conditions at the depositional site of the Siqeifa 1X well, which fits with our interpreted deltaic setting. In the dysoxic–anoxic marginal marine facies, the formation of pyrite within lignite/carbonaceous material is related to the fluvial supply of detrital iron minerals commonly associated with high influxes of terrestrial organic matter into the brackish water, where bacterial sulphate reduction is an active process (Einsele, 1992; Tyson, 1995; Singh et al., 2017a).

The occurrence of glauconite along with carbonaceous material in samples from 7250 ft (2209.8 m) and 6050 ft (1844 m) of the Kharita Formation also indicates a marine influence

(Einsele, 1992; Dooley, 2006), which is further supported by the occurrence of open marine dinoflagellate cysts, for example *Oligosphaeridium* and *Florentinia* (Prauss, 2006; Carvalho et al., 2016; Deaf and Tahoun, 2018). Although the Abu Tunis 1X and Siqeifa 1X wells both being characterized by deltaic deposition, the Kharita Formation in Abu Tunis was deposited in relatively deeper deltaic to more distal shallow marine settings, as indicated by the open marine, middle shelf dinoflagellate cyst *Oligosphaeridium* in Abu Tunis, where the latter was recently found to tolerate low salinity conditions (Deaf and Tahoun, 2018). Conversely, the dinoflagellate cyst assemblages in Siqeifa 1X are composed mainly of the restricted (brackish) forms (*Subtilisphaera, Odontochitina*) with few open marine forms (*Oligosphaeridium* and *Florentinia*). The PMI values are higher in the Abu Tunis 1X well by comparison to those in the Siqeifa 1X well, which also supports an interpretation of relatively more offshore/deeper conditions in the Abu Tunis area (figs. 8 and 9). To summarize, it is suggested that more reducing conditions developed at the relatively more offshore/deeper settings of the Abu Tunis 1X well, resulting in preservation of more organic-rich deposits in comparison to the less reducing conditions that prevailed at the more marginal depositional setting of the Siqeifa 1X well on the eastern margin of Matruh Basin.

4.3. Organic geochemistry and petrography for organofacies detection

The combination of organic geochemical and TWL petrographic analysis (mainly palynofacies) is widely accepted among organic geochemists as a better tool used for recognizing organic facies and hydrocarbon source potential than using the kerogen type alone (Tyson, 1995; Mendonça Filho et al., 2012). This is because organic facies combined with the kerogen type reflect the source and depositional settings that control sedimentation and preservation of organic matter in a potential source rock (e.g., Tyson, 1995). Several definitions of 'organic facies' have been suggested (see Tyson, 1995; Mendonça Filho et al., 2012; Abarghani et al., 2018; and references therein). For example, Pepper and Corvi (1995, p. 297-298) defined an organofacies as "a collection of kerogens derived from common organic precursors, deposited under similar environmental conditions and exposed to similar to early diagenetic histories". They proposed six organofacies based on the kerogen type, principal biomass, sulphur content, and depositional environment. However, Jones (1987) provided a classification of organic facies, which is primarily based on the organic geochemical parameters and takes into account the AOM as one of the main contributors to the organic matter, and hence provides a better identification of the organic facies. The above classification is recognized as a very practical tool because it discriminates the stratigraphic units successfully (e.g., Pasley, 1991; Tyson, 1995; Mendonça Filho et al., 2012). Later, Tyson (1995) provided a definition of the organic facies as "'a body of sediment containing a distinctive assemblage of organic constituents, which can either be recognized by microscopy, or is associated with a characteristic bulk organic geochemical composition". In this sense, Tyson (1995, p. 378) presented a modified model of Jones (1987), where he integrated the palynofacies kerogen parameters and the important environmental parameters with the pyrolysis-estimated organic geochemical parameters. The focus of the current study is to present detailed organic petrographic (TWL, RWL, and UV), palynofacies, and geochemical examinations of the organic matter of the Kharita Formation. Thus, the Jones (1987) model and the modified model of Tyson (1995) will be used here because they employ integrated organic petrographic and geochemical analyses, providing a better identification of the organic facies. In addition, these models provide supporting evidence on the source of the sedimentary organic matter and the environmental controls on sedimentation and preservation of the organic matter, which have been already interpreted in the previous section 4.2.

It is important to note that the deltaic deposits show strong vertical fluctuations in sedimentation (i.e., between regressive and transgressive), where repeated deposition of alternations of organic-rich, fine-grained and organic-poor, coarse-grained clastics is common (Einsele, 1992; Boggs, 2006). Here, source rock evaluation will be based primarily on the palynofacies units identified. As a result, the organic petrographic, geochemical and palynofacies units are used to define organofacies units according to the nature and type of organic matter and its organic geochemical parameters. This approach is consistent with the definitions of the organofacies of Jones (1987) and Tyson (1995).

Rock-Eval pyrolysis of the Abu Tunis 1X well samples indicates a mixture of kerogen types dominated by Type III along with subsidiary Type II for the entire Kharita Formation (HI: 126–389.3, avg. 213.9 mg HC/g TOC; Fig. 10, Table 1). A plot of the different PM constituents in the Abu Tunis 1X well in the LVI ternary diagram of Dow (1982) shows that the samples are rich in oil-prone liptinite macerals and gas-prone vitrinite macerals, and poor in inertinite macerals (Fig. 11a, Table 5). TWL petrography and palynofacies analysis of the organic matter show a palynofacies (PF) unit, which is generally dominated by AOM and non-opaque phytoclasts (Fig. 8, Table 5). This palynofacies is subdivided into two sub-palynofacies units, namely PF-1A and PF-1B, based on the higher abundances of terrestrial or marine palynomorphs (Table 3). PF-1A is found in the frequent shale and argillaceous sandstone alternations of the lower Kharita Formation (depths 7300–6450 ft/2225–1966 m), where the shale intervals are rich in organic matter, and is dominated by AOM (43.4–91, avg. 70.2 %) and subordinate translucent phytoclasts (3.8–47.6, avg. 21.4 %; Fig. 8, Fig. 12a, and Table 5). PF-1A also contains high abundances of terrestrial palynomorphs (90.7–100, avg. 97.4 %), and very low frequencies of opaque phytoclasts (1.6–10.2, avg. 5 %) and marine palynomorphs (0.3–9.3, avg. 2.8 %). Palynofacies, TWL petrographic characterization, average HI (246.6 mg HC/g TOC) and OI (100 mg HC/g TOC) values of the shale intervals indicate a mixture of kerogen Types II and III (Baskin, 1997) in the organic-rich suboxic–anoxic deltaic facies of the lower Kharita. This generally corresponds to the organofacies BC (mixed kerogen Types II/III) of Jones (1987) and Tyson (1995), which produces mainly oil and less gas (Tyson, 1995; Baskin, 1997). The low HI values (183.9–258.0, avg. 215.6 mg HC/g TOC) and AOM (60–87.6, avg. 66 %) and relatively high non-opaque phytoclast frequencies (3.8–33.2, avg. 25.2 %) of the lower PF-1A shale intervals at depths 7300–6850 ft/2225–2088 m (excepting at 6900 ft/2103.1 m) suggest a gas-prone organofacies C (kerogen Type III). However, the relatively higher HI values (228.4–389.3, avg. 282.8 mg HC/g TOC) and AOM (43.4–91, avg. 75.4 %) and the lower non-opaque phytoclast frequencies (5.4–47.6, avg. 16.6 %) of the shale intervals of the upper PF-1A (depths 6849.9–6450 ft/2088–1966 m) suggest oil/gas-prone organofacies BC (mixed kerogen Types II/III).

PF-1B is found in the shale and argillaceous sandstone alternations and the carbonate units of the upper Kharita Formation (depths 6449.9–5600 ft/1965.9–1707 m), which are notably less rich in organic matter in comparison to PF-1A (Fig. 8). PF-1B shows an increase in the frequencies of non-opaque phytoclasts (23.6–70, avg. 43.3 %) at the expense of AOM (19.6–69, avg. 46.2 %; Fig. 8, Fig. 12b, and Table 5). PF-1B is relatively enriched in opaque phytoclasts (3–12, avg. 7.4 %) and marine palynomorphs (0.2–16, avg. 6.8 %), and shows a relative decrease in terrestrial palynomorphs (84–98, avg. 93.2 %). PF-1B also spans the stratigraphic interval with frequent occurrences of bulk coaly carbonaceous material in the shale and argillaceous sandstone intervals of the upper Kharita Formation (Fig. 8). Sampled shale and carbonate intervals of PF-1B (excepting the organic-lean sand and carbonate samples at depths 6100 ft/1859.3 m, 6050 ft/1844 m, 5800 ft/1767.8 m and 5600 ft/1706.9 m) show comparatively lower HI (125.9–250, avg. 181 mg HC/g TOC) and higher OI (104.8–201.2, avg. 158.5 mg HC/g TOC) values similar to those of PF-1A. This indicates a mixture of kerogen Types II and III (Baskin, 1997) for the relatively less organic, suboxic–anoxic deltaic–shallow marine facies of the upper Kharita Formation. Palynofacies, organic petrographic and geochemical characterizations of the PM of the shale and carbonate intervals of PF-1B show insignificant vertical changes and indicate organofacies C (mixed kerogen Types II/III) of Jones (1987) and Tyson (1995), prone to produce mainly gas and less oil (Tyson, 1995; Baskin, 1997).

RWL petrography of the kerogen constituents of PF-1A of the lower Kharita Formation indicates that the vitrinitic maceral group (kerogen Type III) is represented by hydrogen-rich, dark-grey vitrinite and telovitrinite (Figs. 13a, f). The liptinite maceral group (kerogen Type II) is represented by marine unicellular telalginite (Fig. 13b), brown-coloured diffuse bituminite (Fig. 13c), bituminite lamellae (Fig. 13d), and minor amounts of cutinite, sporinite and lamalginite. The inertinite maceral group (kerogen Type IV) is represented by rare fusinite (Fig. 13e). Incident UV analysis of the DOM of the the lower Kharita Formation shows weak dull-yellow fluorescence of telalginite (Fig. 14a, c), cutinite (Fig. 14d), and weak fluorescence of bituminite/AOM, visible at the top of Fig. 14c. This maceral composition confirms the mixture of kerogen Types III and II (Tyson, 1995).

RWL petrography of the kerogen constituents of PF-1B of the upper Kharita Formation shows a maceral composition similar to the lower Kharita Formation, including telovitrinite (Fig. 15a), H-rich vitrinite (Fig. 15b), telalginite (Fig. 15c), bituminite lamellae (Fig. 15d), and ovalshaped brown-coloured bituminite (Fig. 15e). Incident UV light shows telalginite having a golden-yellow fluorescence colour (Fig. 15f).

The LVI ternary plot of the different PM (kerogen) constituents in the Siqeifa 1X well shows that the samples are rich in gas-prone vitrinite macerals, less rich in oil-prone liptinite macerals, and very poor in inertinite macerals (Fig. 11b, Table 7). TWL petrography shows a palynofacies different from that recorded from the Abu Tunis 1X well, which is dominated by non-opaque phytoclasts and contains subordinate AOM frequencies (Fig. 9, Table 7), here referred to as PF-2 and subdivided into two sub-palynofacies - PF-2A and PF-2B - based on the frequency of terrestrial and marine palynomorphs. PF-2A corresponds to the alternations of shale, bulk coaly carbonaceous and argillaceous sandstone horizons, and the argillaceous dolostone interval of the lower Kharita Formation (depths 7400–7000 ft/2255.5–2133.6 m), which are less rich in organic matter in comparison to the Abu Tunis 1x well (Fig. 9). PF-2A is enriched in terrestrial organic matter (non-opaque phytoclasts), and also has lower marine palynomorph frequencies (1.67–4, avg. 2.67 %) when compared to those of PF-1A and PF-1B of Abu Tunis and to those of PF-2B of Siqeifa 1X (figs. 8 and 9, tables 3 and 4). PF-2A is dominated by non-opaque phytoclasts (54.6–63, avg. 59 %) and AOM (32–43, avg. 36 %), with only rare occurrences of opaque phytoclasts (1–2.6, avg. 1.6 %; Fig. 9, Fig. 12c, and Table 7). Samples yielding PF-2A show minor vertical variations in the palynofacies data and organic geochemical parameters (TOC, S_2, HI, OI; Fig. 9, and Table 2) and are thus assigned to a single organofacies unit. The shales and argillaceous dolostones that yield PF-2A show low HI (93–159.2, avg. 128 mg HC/g TOC) and high OI (118.5–257, avg. 176.5 mg HC/g TOC) values, indicating kerogen Type III (Baskin, 1997) in the relatively oxic (dysoxic–anoxic) deltaic shales and argillaceous dolostones of the lower Kharita Formation. Integrated palynofacies, organic petrographic, and geochemical analyses suggest a gas-prone organofacies C (kerogen Type III) of Jones (1987) and Tyson (1995).

PF-2B has been isolated from the upper Kharita Formation (depths 6999.9–5850 ft/2133.5–1783 m), composed mainly of alternations of more frequent bulk coaly carbonaceous and/or argillaceous sandstone and less frequent shale intervals (Fig. 9), and is relatively rich in organic matter and PF-2B shows a relative increase in non-opaque phytoclasts (56–75.4, avg. 67.7 %) at the expense of AOM (18.2–39.4, avg. 25.7 %). Minor enrichment in opaque phytoclasts (1.6–5.4, avg. 3.1 %) and marine palynomorphs (3.3–6.3, avg. 4.8 %) is also recorded in PF-2B (Fig. 9, Fig. 12d, and tables 4 and 7). Samples containing PF-2B show a minor vertical variation in the palynofacies and organic geochemical data (Fig. 9, and Table 2). The shales containing PF-2B show relatively higher HI (107.3–292.7, avg. 170.5 mg HC/g TOC) and lower OI (97.6–199.1, avg. 144.4 mg HC/g TOC) values in comparison to those of PF2A. However, two samples (out of 17) show an HI of 292.7 and 250.7 mg HC/g TOC (i.e., organofacies BC = mixed kerogen Types II/III). These data indicate a dominance of kerogen Type III (Baskin, 1997) in the relatively oxic (dysoxic–anoxic) deltaic shales of the upper Kharita Formation. Shale and argillaceous sandstone samples yielding PF-2B are characterized by the occurrence of some stringers of lignite and frequent bulk coaly carbonaceous material (WEPCO, 1970), which corroborates the presence of gas-prone kerogen Type III material (Mendonça Filho et al., 2012; Singh et al., 2017b). In addition, at least some of the AOM particles in PF-2A can be identified as originating from bacterially degraded non-opaque phytoclasts, as some AOM shows relict structure of phytoclast outlines but with irregular and diffuse edges, and also contain pyrite specked and inclusions (Fig. 12d). Thus, these terrestrially derived AOM particles can also be identified as Type III kerogen (e.g., Tyson, 1995; Singh et al., 2017b). The combined palynofacies, organic petrography, and geochemistry data of PF-2B indicate a gas-prone kerogen Type III-dominated organic facies for the shale intervals of the upper Kharita Formation.

RWL analysis of kerogen constituents of PF-2A shows that the liptinite maceral group is represented by telalginite (Fig. 16a–b) and sporinite (Fig. 16c–d). The vitrinite maceral group is represented by telovitrinite (Fig. 16e) and H-rich vitrinite (Fig. 16f). The kerogen constituents of PF-2B indicate that the liptinite maceral group is composed of *Tasmanites* telalginite (Fig. 17a), sporinite (Fig. 17c, e) and cutinite (Fig. 17f). The vitrinite group consists of telovitrinite (Fig. 17e) and the inertinite maceral group is represented by fusinite (Fig. 17d). Traces of spherical bituminite are also present (Fig. 17b). Reflected UV light analysis shows the presence of sporinite (Fig. 18a, b), which exhibits a yellow fluorescence colour.

4.4. Organic maturation

The organic matter of the Kharita Formation in the Abu Tunis 1X well is immature to marginally mature, based on the Tmax values (all are in the 415–426 °C) and confirmed by measured vitrinite reflectance (%Rv is in the 0.48–0.57 range) - although the sample at 7050 ft (2149 m) may have reached the early oil-window stage (Fig. 19). It can therefore be anticipated that intervals of the Kharita Formation present deeper in the Matruh Basin will have higher thermal maturity and have evolved further into the oil-window (Metwalli et al., 2018). These data are in good agreement with the TAI (2 to 2+) obtained from TWL petrography of smooth pteridophyte spores. Examination of the UV fluorescence of the DOM shows orange-yellow and dull-yellow colours of the liptinite macerals (sporinite and lamalginite) in the lower Kharita, to greenish-yellow (lamalginite) in the upper Kharita, which indicates an immature to early upper mature phase (Mukhopadhyay, 1994). The organic matter in the Kharita Formation of the Siqeifa 1X well is slightly more mature than in the Abu Tunis 1X well based on the consistently higher Tmax (421–432 °C) and measured %Rv values (0.48–0.59). The UV excitation of the DOM shows orange-yellow sporinite and lamalginite colours, which indicates peripherally an immature to mainly early upper mature phase (Mukhopadhyay, 1994).

4.5. Hydrocarbon source rock evaluation

The deltaic deposits of the lower Kharita Formation in the Abu Tunis 1X well contain considerable organic-rich intraformational shale intervals, which comprise a total content of about 13.2 % and range in thickness from 1.5 to 9.8 m, comprise about 34 m net source rock, and show remarkable intraformational variations in organic richness, which range from good to very good/excellent. Combining these factors indicates that the lower Kharita Formation should be considered as a significant hydrocarbon source with very good to excellent hydrocarbon potential (Fig. 20a). This interpretation is consistent with several hydrocarbon exploration studies, where organic-rich intraformational intervals of similar net source thickness were deemed to have important hydrocarbon source rock potential (e.g., Katz et al., 2000; Hakimi and Abdullah, 2014). Shale intervals in the lower part of the lower Kharita Formation are particularly rich in terrestrially sourced organic matter (i.e., gas-prone), while those in the upper part are rich in marine and terrestrially sourced organic matter (i.e., oil and gas-prone). However, the immature to early upper thermal maturity and the oil-cross over (Fig. 20b) indicate a low probability for the lower Kharita shales to produce oil (avg. generated oil in rock from pyrolysis is 81.8 bbl oil/ac–ft; Table 1) with no gas production (Fig. 8). The intraformational argillaceous sandstones are poor in organic matter and regarded as reservoir intervals. In contrast, the deltaic–shallow marine deposits of the upper Kharita Formation contain fewer organic-rich intraformational shale and carbonate intervals, with the former (between 3.7 and 12.2 m thick) comprising a net source rock interval of about 9.8 % (25.3 m), whereas limestone and dolostone intervals (6.7 to 39.6 m thick) comprise a greater net source rock interval of about 23.4 % (60.6 m). The shale and carbonate intervals collectively comprise in total a total net source rock interval of about 33.2 % (86 m) with little intraformational variation in organic richness. The thicker organic-rich intervals show low potential as oil source rocks but fair to good potential as gas sources due to enrichment of the gas-prone coaly carbonaceous material, which could represent another important hydrocarbon source. However, these deposits are still not sufficiently thermally mature to produce appreciable quantities of either oil or gas. The argillaceous and/or carbonaceous sandstones of the upper Kharita Formation have very low organic matter content and thus are defined as reservoir horizons.

Lateral intrabasinal variation in lithofacies, organic facies, and organic richness can be demonstrated in the Kharita Formation, as on the eastern margin of the Matruh Basin in the Siqeifa 1X area, there is a higher average shale content (34.2 %) than in the Abu Tunis 1X well (23 %) according to WEPCO (1968, 1970). However, the deltaic shales of the lower Kharita Formation of Siqeifa 1X are less organic-rich (23.7 %, 29 m thick net source rock) as is the shaley dolostone (7 %, 8.5 m thick). However, these Siqeifa 1X intervals are rich in terrestrially sourced organic matter and show little intraformational variation in organic richness, and have been shown to have fair to good gas-prone source rock potential (Fig. 20a). The argillaceous and carbonaceous sandstones of the lower Kharita Formation are organic-lean and are considered reservoir intervals. Vertical lithofacies and organic richness can be seen in the deltaic upper Kharita Formation as shale intervals become less frequent (12.1 %) and their thicknesses reduce (2.7–6.7 m). Nevertheless, these upper Kharita shales show relatively high organic richness due to deposition of coals and coaly carbonaceous material, but only have a fair to good to less very good gas-prone source rock potential. This lateral diminishing in the kerogen quality and richness of the Kharita Formation between Abu Tunis 1X and Siqeifa 1X results from the latter being deposited in a relatively oxygenated deltaic environment, where significant preservation of AOM and deposition of coal is less likely (Tyson, 1995; Mendonça Filho, et al., 2012). The immature to early upper stage of thermal maturity and the oil cross-over (Fig. 20b) indicates a very low probability for the shale intervals of the entire Kharita Formation in the Siqeifa 1X to produce oil (avg. generated oil in rock from pyrolysis is only 11.76 bbl oil/ac–ft) and would produce no gas (Table 2). The argillaceous sandstone and dolostone deposits of the upper Kharita Formation have reservoir characteristics.

Against this, recent seismic structural analysis and basin modelling of the sedimentary sequence in the Matruh Basin revealed more mature potential gas-prone source rocks of the Kharita Formation to the southeast of the Abu Tunis 1X and Siqeifa 1X wells (Metwalli et al., 2018). The latter authors constructed a maturity map and a thermal history model of the Kharita Formation, based on measured well-bottom temperatures to the SE of our study wells. In this maturity map, the Abu Tunis 1X and Siqeifa 1X wells showed relatively higher maturity levels (early mature) of 0.60-0.70 %Rv in comparison to our current determination 0.48 and 0.57 %. Despite this difference in measured and calculated values, the general increase in maturity in an eastward direction consistent with maturation we record at Siqeifa 1X. The Kharita Formation in the Mideiwar 1X, Matruh 1-1, Matruh 2-1, and Matruh 3-1 wells in Matruh Basin show shale contents of 21.7 %, 22.1 %, 21.4 %, and 23.2 % similar to that recoded from the Abu Tunis 1X (23 %), but with a relatively higher maturity level (Metwalli et al., 2018; see Fig. 21). The burial and thermal history modelling of Metwalli et al. (2018) on the Kharita Formation indicates the presence of more mature (late mature, oil-window and main gas generation, 1–1.3 %Rv) potential gas-producing zones to the east and southeast of our studied area of the basin. This is specifically shown in the Darduma 1A, Matruh 1-1 and Ras Kanayes wells (Fig. 21).

5. Conclusions

Previously the Albian Kharita Formation has been understood to possess very little hydrocarbon source rock potential in the Shushan and Sidi Barani basins, and was effectively viewed as only a hydrocarbon reservoir unit. However, high organic matter influxes and reducing conditions at the more offshore/deeper setting of the Abu Tunis 1X well in the Matruh Basin resulted in better preservation of organic-rich, intraformational shale and carbonate deposits. In this paper we have demonstrated that in the Abu Tunis 1X well the lower Kharita Formation is a good to very good/excellent potential hydrocarbon source rock, although in the less reducing conditions that prevailed at the eastern margin of Matruh Basin at the Siqeifa 1X well produced lower organic content and lower source rock potential.

Our integrated organic geochemical, organic petrographic, and palynofacies analyses indicate that the deltaic–shallow marine shales and minor carbonates of the Kharita Formation in the Abu Tunis 1X well comprise significant net source rocks of about 120 m thickness. The lower Kharita Formation in particular contains 34 m net shale source rock and shows good to very good/excellent gas and oil/gas potential (1.14–11.59 TOC wt %; S_2: 2.72–23.53 mg HC/g). The shales and carbonates of the upper Kharita also comprise another important hydrocarbon source with a thicker net source rock interval of 86 m, but they are less organic-rich and show only fair to good) gas/oil source rock potential (0.82–1.78 TOC wt %; S_2: 1.07–4.02 mg HC/g). Although the entire Kharita Formation in the Abu Tunis area contains important source rock intervals, in terms of thermal maturity these intervals are immature to marginally mature. In the Siqeifa 1X well, the deltaic intraformational shale and shaley dolostone deposits are less organic-rich, but comprise a considerable net source rock of about 80 m thickness, with an overall fair to good to less very good gas source rock potential (0.81–2.14 TOC wt %; S_2: 0.88–4.80 mg HC/g), and ranges from immature to marginally mature. The frequent shale and minor carbonate intervals of the Kharita Formation at the depocentre of the Matruh Basin (i.e., Abu Tunis 1X) are very rich in gas/oil-prone organic matter, while the shale and minor shaley dolostone intervals of the Kharita Formation at the basin margin (e.g., Siqeifa 1X) are rich in gas-prone organic matter. It has been shown that the lithofacies, organic facies/richness and organic quality vary laterally across the basin, and therefore so does the hydrocarbon potential of the Kharita Formation.

Previously often ignored, we have demonstrated that the shales within the Kharita Formation possess suitable organic richness and source rock potential, and therefore in the future this unit will be of more interest in terms of hydrocarbon prospectivity because of its regional subsurface extent across northwestern Egypt (Tahoun et al., 2017). Although the Kharita Formation at both of our study sites is too thermally immature to have produced oil or gas, this formation may contain more mature organic matter that has reached the late mature oil- to main gas-generation window in the more eastern and southeastern parts of the Matruh Basin where higher thermal maturities have been modelled (Metwalli et al., 2018), and is thus a prime exploration target.

Figure captions

Fig. 1: Map showing the location of the Matruh Basin, the Abu Tunis 1X and Siqeifa 1X wells, and a simple structural map of the basin (modified after EGPC, 1992; Shalaby et al., 2012).

Fig. 2: Generalized lithostratigraphic column, showing chronostratigraphy, depositional environments, and the petroleum system of the sedimentary sequences in the Matruh Basin, north Western Desert, Egypt (after Aram et al., 1988; EGPC, 1992).

Fig. 3: Quantitative distribution of palynomorphs and particulate organic matter (in grains/gram), showing six fine-grained clastic organic-rich intervals within the Kharita Formation (after Deaf, 2009).

Fig. 4: Scheme of the protocol employed in this paper for the analysis of hydrocarbon potential.

Fig. 5 (A) Plot of the total organic carbon content (TOC) against depth, showing the organic richness of the Kharita Formation in the Abu Tunis 1X and Siqeifa 1X wells. (B) Plot of the oil potential versus S_2, showing the hydrocarbon potential of the Kharita Formation in the Abu Tunis 1X and Siqeifa 1X wells. (C) Plot of S_2 against TOC showing the hydrocarbon source rock potential of the Kharita Formation in the Abu Tunis 1X and Siqeifa 1X wells.

Fig. 6: Spores–Microplankton–Pollen (SMP) ternary plots showing depositional environments of the Kharita Formation (after Federova, 1977; Duringer and Doubinger, 1985). (A) SMP plot of the Abu Tunis 1X well samples. (B) SMP plot of the Siqeifa 1X well samples.

Fig. 7: AOM–Phytoclasts–Palynomorphs (APP) ternary plots showing different palynofacies types and redox conditions for the Kharita Formation (after Tyson, 1995). (A) APP plot of the Abu Tunis 1X well samples. (B) APP plot of the Siqeifa 1X well samples.

Fig. 8: Chart showing lithologic column, organic petrographic and geochemical data, and the hydrocarbon potential of the Kharita Formation in the Abu Tunis 1X well.

Fig. 9: Chart showing lithologic column, vertical stratigraphic distributions of palynofacies parameters, suggested depositional environments, organic petrographic and geochemical data, and the hydrocarbon potential of the Kharita Formation in the Siqeifa 1X well.

Fig. 10: Pseudo-Van Krevelen diagram showing kerogen types in the Kharita Formation in the Abu Tunis 1X and Siqeifa 1X wells.

Fig. 11: Liptinite–Vitrinite–Inertinite (LVI) ternary kerogen plots (after Dow, 1982; Tyson, 1995) showing the hydrocarbon source rock potential of the Kharita Formation. (A) LVI plot of the Abu Tunis 1X well samples, (B) LVI plot of the Siqeifa 1X well samples.

Fig. 12: Representative palynofacies assemblages from the Kharita Formation. Key to labels: Sp = spore, Sp-Pyr = spore filled with pyrite, N-OP = non-opaque phytoclast, De N-OP = degraded non-opaque phytoclast, OP = opaque phytoclast, AOM (De N-OP) = AOM of probably degraded N-OP phytoclast origin, MbT = membranous tissue. (A) PF-1A (AOM/phytoclast-dominated) with abundant spores from the lower Kharita Formation in the Abu Tunis 1X well, sample depth (7000a ft/2133.6 m) at x250 magnification. (B) PF-1B (AOM/phytoclast-dominated) with abundant black wood from the upper Kharita Formation in the Abu Tunis 1X well, sample depth (6300b ft/1920.2 m) at x250 magnification. (C) PF-2A (Phytoclast/AOM-dominated) with abundant spores from the lower Kharita Formation in the Siqeifa 1X well, sample depth (7350a ft/2240.3 m) at x250 magnification. (D) PF-2B (Phytoclast/AOM-dominated) with abundant spores from the upper Kharita Formation in the Siqeifa 1X well, sample depth (5850a ft/1783 m) at x250 magnification.

Fig. 13: Photomicrographs of dispersed organic matter (DOM) in PFA-1, Abu Tunis 1X well, taken under reflected white light. (a) Hydrogen-rich vitrinite, depth 7000 ft (2133.6 m); (b) Telalginite, depth 7000 ft; (c) Light-brown bituminite, depth 7000 ft; (d) Bituminite lamellae, depth 7000 ft; (e) Fusinite with compressed cell lumens, depth 5750 ft (1752.6 m); and (f) Telovitrinite, depth 6600 ft (2011.7 m).

Fig. 14: Photomicrographs of dispersed organic matter (DOM) in the Abu Tunis 1X well (6900 ft/2103 m) taken under reflected UV light. Excitation is at 465 nm; combined dichroic mirror and

barrier filter have a long pass at 515 nm. (a) Telalginite; (b) Sporinite; (c) Telalginite; and (d) Cutinite.

Fig. 15: Photomicrographs of dispersed organic matter (DOM) in PFA-2, Abu Tunis 1X well, taken under reflected white light. (a) Telovitrinite, depth 6400 ft; (b) Hydrogen-rich vitrinite, depth 5750 ft (1752.6 m); (c) Telalginite being converted to bituminite, depth 5850 ft (1783 m); (d) Bituminite lamellae, depth 6400 ft (1950.7 m); (e) Bituminite depth 6250 ft (1905 m); and (f) Lamalginite depth 5850 ft (1783 m). Photomicrograph (e) was taken under reflected UV light using the same filters as in Fig. 13.

Fig. 16: Photomicrographs of dispersed organic matter (DOM) in PF2-A, Siqeifa 1X well, taken under reflected white light. (a) *Tasmanites* telalginite, depth 6450 ft (1966 m); (b) Telalginite, depth 6450 ft; (c) Sporinite showing the characteristic trilete mark, depth 7000 ft (2133.6 m); (d) Sporinite, depth 7000 ft; (e) Telovitrinite, depth 7300 ft (2225 m); and (f) H-rich vitrinite, depth 7100 ft (2164 m).

Fig. 17: Photomicrographs of dispersed organic matter (DOM) in PF2-B, Siqeifa 1X well, taken under reflected white light. (a) Telalginite, depth 6300 ft (1920 m); (b) Spherical bituminite, depth 6300 ft; (c) Sporinite (pollen grain showing two possible elater-like appendages), depth 5850 ft (1783 m); (d) Inertinite, depth 5850 ft (1783 m); (e) Telovitrinite enclosing compressed sporinite, depth 6150 ft (1874.5 m); and (f) Cutinite in transverse section showing the characteristic ‘teeth’ (arrows), depth 6150 ft.

Fig. 18: Photomicrographs of dispersed organic matter (DOM) in the Siqeifa 1X well taken under reflected UV light from a depth of 5700 ft (1737 m). (a) Sporinite (pollen grain showing at least two elater-like appendages) arrows point to the two appendages (Ap); (b) Sporinite (spore).

Fig. 19: Plot of HI versus Tmax showing kerogen types and thermal maturation levels for the Kharita Formation in the Abu Tunis 1X and Siqeifa 1X wells.

Fig. 20: (A) Kerogen quality diagram showing potential kerogen types of the Kharita Formation in the Abu Tunis 1X and Siqeifa 1X wells. (B) Oil cross-over diagram showing a low probability of both the Abu Tunis 1X and Siqeifa 1X wells to generate oil.

Fig. 21: Map showing the different maturity levels at the surface of the Kharita Formation across Matruh Basin (modified after Metwalli et al., 2018), the recorded maturation of the Abu Tunis 1X and Siqeifa 1X wells, and the potential promising hydrocarbon wells in the basin. Arrow points to the potential promising mature source rocks in the basin.

Disclosure of interest

The authors declare that they have no competing interest.

Acknowledgements

We are grateful for the Egyptian General Petroleum Corporation (EGPC) for providing samples and well log upon which the present work was based. Thanks also go to the Editor-in-Chief Dr. Max Qinhong, Associate Editor Dr. Hui Tian, and the two anonymous reviewers for their critical review and constructive comments.

ORCID ID

Amr Deaf, http://orcid.org/0000-0002-5073-7911

Ian C. Harding, http://orcid.org/0000-0003-4281-0581

John Marshall http://orcid.org/0000-0002-9242-3646

References

Abarghani, A., Ostadhassan, M., Gentzis, T., Carvajal, H., Bubach, B., 2018. Organofacies study of the Bakken source rock in North Dakota, USA, based on organic petrology and geochemistry. Int. J. Coal Geol. 188, 79–93.

Abdel Halim, M., Moussad, M., 1992. Western Desert Oil and Gas fields (a comprehensive overview). Proceedings of the 11th Petroleum Exploration and Production Conference (E.G.P.C. 92): 432.

Aboul Ela, N., Tahoun, S.S., Fouad, T., Mousa, D.A., Saleh, R., 2018. Source rock evaluation of Kharita and Bahariya formations in some wells, North Western Desert, Egypt: Visual palynofacies and organic geochemical approaches. Egypt. J. Pet. 27, 455–465.

Abrams, M.A., Greb, M.D., Collister, J.W., Thompson, M., 2016. Egypt far Western Desert basins petroleum charge system as defined by oil chemistry and unmixing analysis. Mar. Pet. Geol. 77, 54–74.

Alaug, A.S., Mahmoud, M.S., Deaf, A.S., Al-Ameri, T.K., 2014. Palynofacies, organic geochemical analyses and hydrocarbon potential of some Upper Jurassic-Lower Cretaceous rocks, the Sabatayn-1 well, Central Yemen. Arab. J. Geosci. 7, 2515–2530.

Aram, R.B., Roehl, N.L., Feazel, C.T., 1988. Seismic stratigraphy and subsurface geology of the north–central portion of the South Umbarka Concession, Western Desert, Egypt. Phillips Petroleum Company Report (11 pp.).

ASTM D2797/D2797M-09, 2007. Standard Practice for Preparing Coal Samples for Microscopical Analysis by Reflected Light. ASTM International, West Conshohocken, PA, pp. 2007. http://dx.doi.org/10.1520/D2797_D2797M-09.

ASTM D7708-14, DATE Standard Test Method for Microscopical Determination of the Reflectance of Vitrinite Dispersed in Sedimentary Rocks, ASTM International, West Conshohocken, PA, 2014, www.astm.org

Baskin, D.K., 1997. Atomic H/C ratio of kerogen as an estimate of thermal maturity and organic matter conversion. AAPG Bull. 81, 1437–1450.

Batten, D.J., 1974. Wealden palaeoecology from the distribution of plant fossils. Proceed. Geol. Assoc. 85, 433–58.

Batten, D.J., 1982. Palynofacies, palaeoenvironments, and petroleum. J. Micropalaeontol. 1, 107–114.

Batten, D.J., 1996. Palynofacies and Palaeoenvironmental Interpretation. In: Jansonius, J., McGregor, D.C. (Eds.), Palynology: Principles and Applications. AASP Found. 3, pp. 1011–1064.

Batten, D.J., Stead, D.T., 2005. Palynofacies analysis and its stratigraphic application. In: Koutsoukos, E.A.M. (Ed.), Applied Stratigraphy. Springer Dordrecht, Netherlands, pp. 203–226.

Behar, F., Beaumont, Y., De, B., Penteado, H.I., 2001. Rock-Eval 6 technology: performances and developments. Oil and Gas Science and Technology. Review Institut Français du Pétrole Energ. Nouv. 56, 111–134.

Ben Fadhel, M., Layeb, M., Hedfi, A., Ben Youssef, M., 2011. Albian oceanic anoxic events in northern Tunisia: Biostratigraphic and geochemical insights. Cret. Res. 32, 685–699.

Boggs, S., 2006. Principles of Sedimentology and Stratigraphy. Pearson Prentice Hall, New Jersey.

Bombardiere, L., Gorin, G.E., 2000. Stratigraphical and lateral distribution of sedimentary organic matter in Upper Jurassic carbonates of SE France. Sediment. Geol. 132, 177–203.

Bornemann, A., J. Pross, K. Reichelt, J. O. Herrle, C. Hemleben, and J. Mutterlose, 2005. Reconstruction of short-term palaeoceanographic changes during the formation of the Late Albian ‘Niveau Breistroffer’ black shales (oceanic anoxic event 1d, SE France). J. Geol. Soc. 162, 623–639.

Bujak, J.P., Barss, M.S., Williams, G.L., 1977. Offshore east Canada's organic type and color and hydrocarbon potential. Oil Gas J. 75, 198–201.

Carvalho, M.A., Mendonça Filho, J.G., Menezes, T.R., 2006. Paleoenvironmental reconstruction based on palynofacies analysis of the Aptian-Albian succession of the Sergipe Basin, Northeastern Brazil. Mar. Micropaleontol. 59, 56–81.

Carvalho, M.A., Bengtson, P., Lana, C.C., 2016. Late Aptian (Cretaceous) paleoceanography of the South Atlantic Ocean inferred from dinocyst communities of the Sergipe Basin, Brazil. Paleoceanography 31, 2–26.

Deaf, A.S., 2002. Palynological Studies on some Cretaceous rocks in northern Egypt. Unpubl. MSc Thesis, Assiut Uni. 220p.

Deaf, A.S., 2009. Palynology, palynofacies and hydrocarbon potential of the Cretaceous rocks of northern Egypt. Publ. PhD, Uni. Southampton 348p. Available online at: https://www.eprints.soton.ac.uk/168943/.

Deaf, A.S., Tahoun, S.S., 2018. Integrated palynological, organic geochemical, and sequence stratigraphic analyses of the middle to upper Cenomanian hydrocarbon reservoir/ source Abu Roash “G” Member: a depositional model in northwestern Egypt. Mar. Pet. Geol. 92, 372–402.

Deaf, A.S., Harding, I.C., Marshall, J.E.A., 2014. Cretaceous (Albian–? early Santonian) palynology and stratigraphy of the Abu Tunis 1X borehole, northern Western Desert, Egypt. Palynology 38, 51–77.

Deaf, A.S., Harding, I.C., Marshall, J.E.A., 2019. Cretaceous (Hauterivian–Cenomanian) palaeoceanographic conditions in southeastern Tethys (Matruh Basin, Egypt): implications for the

Cretaceous climate of northeastern Gondwana. Cret. Res.; DOI: https://doi.org/10.1016/j.cretres.2019.104229

Degens, E.T., Mopper, K., 1976. Factors controlling the distribution and early diagenesis of organic material in marine sediments. In: Riley, J.P., Chester, R. (Eds.), Chemical Oceanography. 2nd ed. London, Academic Press 6, pp. 59–113.

Dembicki, H., 2009. Three common source rock evaluation errors made by geologists during prospect or play appraisals. AAPG Bull. 93, 34–356.

Dembicki, H., 2016. Practical Petroleum Geochemistry for Exploration and Production. Elsevier, Amsterdam.

Dooley, J.H., 2006. Glauconite. In: Kogel, J.E., Trivedi, N.C., Barker, J.M.,Krukowski, S.T. (Eds.), Industrial Minerals and Rocks, 7th ed. Society of Mining and Metal Exploration, Littleton, pp. 495–506.

Dow, W.G., 1982. Kerogen maturity and type by reflected light microscopy applied to petroleum exploration. In: Staplin, F.L., Dow, W.G., Milner, C.W.O., Milner, C.W.D., O'Connor, D.I., Pocock, S.A.J., van Gijzel, P., Welte, D.H., Yukler, M.A. (Eds.), How to Assess Maturation and Paleotemperatures, SEPM Short Course 7., pp. 133–157.

Duringer, P., Doubinger, J., 1985. La palynologie: un outil de characterisation des facies marines et continentaux a la limite Muschelkalk Supérieur-Lettenkohle. Sci. Géol. Bull., Strasbourg 38, 19–34.

EGPC, 1992. Western Desert, Oil and Gas Fields (A Comprehensive Overview), Cairo, Egypt (431 pp.).

Einsele, G., 1992. Sedimentary Basins: Evolution, Facies, and Sediment Budget. Springer-Verlag, Berlin.

El-Soughier, M.I., Deaf, A.S., Mahmoud, M.S., 2014. Palynostratigraphy and palaeoenvironmental significance of the Cretaceous palynomorphs in the Qattara Rim-1X well, north Western Desert. Egypt. Arab. J. Geosci. 7, 3051–3068.

Espitalié, J., Deroo, G., Marquis, F., 1985. La pyrolyse Rock-Eval etses applications (part I). Rev. Inst. Fr. Pétrol. 40, 563–579.

Federova, V.A., 1977. The significance of the combined use of microphytoplankton, spores, and pollen for differentiation of multi-facies sediments. In: Samoilovich, S.R., Timoshina, N.A. (Eds.), Questions of Phytostratigraphy. Leningrad, Trudy Neftyanoi nauchno-issledovatelskii geologorazvedochnyi Institute (VNIGRI), pp. 70–88.

Firth, J.V., 1993. Palynofacies and thermal maturation analysis of sediments from the Nankai Trough. Proceed. ODP, Sci. Res. 131, 57–69.

Gentzis, T., Carvajal, H., Deaf, A., Tahoun, S.S., 2018. Multi-proxy approach to screen the hydrocarbon potential of the Jurassic succession in the Matruh Basin, North Western Desert, Egypt. Int. J. Coal Geol. 190, 29–41.

Gentzis, T., Carvajal, H., Tahoun, S.S, Deaf, A., Ocubalidet, S., 2019. Organic facies and hydrocarbon potential of the early-middle Kharita Formation in the Abu Gharadig Basin, Egypt as demonstrated by palynology, organic petrology, and geochemistry. Int. J. Coal Geol. 209, 27–39.

Ghorab, M.A., Ebeid, Z., Tawfik, N., 1971. On the stratigraphy of the northeastern corner of the Western Desert. Proceed. 9th Ann. Meet. Geol. Soc. Egypt, Giza, Egypt, p. 48.

Green, O.R., 2001. A manual of practical laboratory and field techniques in palaeobiology. Dordrecht, Kluwer Academic Publishers.

Guiraud, R., Bosworth, W., 1999. Phanerozoic geodynamic evolution of north-eastern Africa and the north-western Arabian platform. Tectonophysics 315, 73–108.

Habib, D., 1983. Sedimentation rate-dependent distribution of organic matter in the North-Atlantic Jurassic-Cretaceous. Init. Rep. DSDP 76, 781–794.

Hackley, P.C., Araujo, C.V., Borrego, A.G., Bouzinos, A., Cardott, B.J., Cook, A.C., Eble, C., Flores, D., Gentzis, T., Gonçalves, P.A., Mendonça Filho, J.G., Hámor-Vidó, M., Jelonek, I., Kommeren, K., Knowles, W., Kus, J., Mastalerz, M., Menezes, T.R., Newman, J., Oikonomopoulos, I.K. Pawlewicz, M., Pickel, W., Potter, J., Ranasinghe, P., Read, H., Reyes, J. Rodriguez, G.D.L.R. , Fernandes de Souza, I.V.A., Suarez-Ruiz, I., Sýkorová, I., Valentine, B. J.,

2015. Standardization of reflectance measurements in dispersed organic matter: Results of an exercise to improve interlaboratory agreement. Mar. Pet. Geol., 59, 22–34.

Hakimi, M.H., Abdullah, W.H., 2014. Source rock characteristics and hydrocarbon generation modelling of Upper Cretaceous Mukalla Formation in the Jiza-Qamar Basin, Eastern Yemen. Mar. Pet. Geol. 51, 100–116.

Hantar, G., 1990. North Western Desert. In: Said, R. (Ed.), The Gelogy of Egypt. Balkema, Rotterdam, pp. 293–319.

Hart, B.S., Steen, A.S., 2015. Programmed pyrolysis (Rock-Eval) data and shale paleoenvironmental analyses: A review. Interpretation 3, SH41-SH58.

Hazra, B., Varma, A.K., Bandopadhyay, A.K., Mendhe, V.A., Singh, B.D., Saxena, V.K., Samad, S.K., Mishra, D.K., 2015. Petrographic insights of organic matter conversion of Raniganj Basin shales, India. Int. J. Coal Geol. 150-151, 193–209.

Helenes, J., Somosa, D., 1999. Palynology and sequence stratigraphy of the Cretaceous of eastern Venezuela. Cret. Res. 20, 447–463.

Herrle, J. O., J. Pross, O. Friedrich, P. Koßler, and C. Hemleben, 2003. Forcing mechanisms for mid-Cretaceous black shale formation: Evidence from the Upper Aptian and Lower Albian of the Vocontian Basin (SE France). Palaeogeogr. Palaeoclimatol. Palaeoecol. 190, 399–426.

International Committee for Coal and Organic Petrology (ICCP), 1998. The new vitrinite classification (ICCP System 1994). Fuel 77, 349–358.

International Committee for Coal and Organic Petrology (ICCP), 2001. The new inertinite classification (ICCP System 1994). Fuel 80, 459–471.

Jones, R.W., (1987). Organic Facies. In: Brooks, J., Welte, D. (Eds.), Advances in Petroleum Geochemistry. Academic Press, London, 2, pp. 1–90.

Katz, B. J., Dittmar, E. I., Ehret, G. E., 2000. A geochemical review of carbonate source rocks in Italy. J. Pet. Geol. 23, 399-424.

Kerdany, M.T., Cherif, O.H., 1990. Mesozoic. In: Said, R. (Ed.), The Geology of Egypt. Balkema, Rotterdam, pp. 407–437.

Khalifa, Z., Affouri, H., Rigane, A., Jacob, J, 2018. The Albian oceanic anoxic events record in central and northern Tunisia: Geochemical data and paleotectonic controls. Mar. Pet. Geol. 93, 145–165.

Lamberson, M.N., Bustin, R.M. and Kalkreuth, W., 1991. Lithotype (maceral) composition and variation as correlated with paleo-wetland environments, Gates Formation, northeastern British Columbia, Canada. Int. J. Coal Geol. 18, 87–124.

Mahmoud, M.S., Deaf, A.S., 2007. Cretaceous palynology (spores, pollen and dinoflagellate cysts) of the Siqeifa 1X borehole, northern Egypt. Riv. Ital. Paleontol. Stratigr. 113, 203–221.

Mahmoud, M.S., Deaf, A.S., Tamam, M.A., Khalaf, M.M., 2017. Palynofacies analysis and palaeoenvironmental reconstruction of the Upper Cretaceous sequence drilled by the Salam-60 well, Shushan Basin: implications on the regional depositional environments and hydrocarbon exploration potential of north-western Egypt. Rev. Micropaleontol. 60, 449–467.

Mahmoud, M.S., Deaf, A.S., Tamam, M.A., Khalaf, M.M., 2019. Revised (miospores-based) stratigraphy of the Lower Cretaceous succession of the Minqar-IX well, Shushan Basin, north Western Desert, Egypt: Biozonation and correlation approach. J. Afr. Earth Sci. 18–35.

Makky, A.F., El Sayed, M.I., Abu El-Ata, A.S., Abd El-Gaied, I.M., Abdel-Fattah, M.I., Abd-Allah, Z.M., 2014. Source rock evaluation of some upper and lower Cretaceous sequences, West Beni Suef Concession, Western Desert, Egypt. Egypt. J. Pet. 23, 135–149.

Mendonça Filho, J.G., 2012. Palynofacies working group. ICCP Meeting, Beijing, pp. 1-24. Available at: http://www.iccop.org/workinggroup/palynofacies/

Mendonça Filho, J.G., Gonçalves, P.A., 2017. Organic matter: concepts and definitions. In: Suárez-Ruiz, I., Mendonça Filho, J.G. (Eds.), Geology: Current and Future Developments. The Role of Organic Petrology in the Exploration of Conventional and Unconventional Hydrocarbon Systems. Bentham Science Publishers, United Arab Emirates, 1, pp. 1–33.

Mendonça Filho, J.G., Menezes, T.R., Mendonça, J.O., et al., 2012. Organic facies: Palynofacies and organic geochemistry approaches. In: Panagiotaras, D. (Ed.) Geochemistry – Earth's system processes. InTech, Rijeka, pp. 211–48.

Meshref, W., 1996. Cretaceous tectonics and its impact on oil exploration in northern Egypt. Geol. Soc. Egypt Spec. Publ. 2, pp. 199–214.

Meshref, W.M., Hammouda, H., 1990. Basement tectonic map of Northern Egypt. Proceedings of the EGPC 9th Exploration and Production Conference 55‐76.

Metwalli, F.I., Pigott, J.D., 2005. Analysis of petroleum system criticals of the Matruh-Shushan Basin, Western Desert, Egypt. Pet. Geosci. 11, 157–178.

Metwalli, F.I., Shendi, E.H., Hart, B., Osman, W.M., 2018. 3D Seismic structural analysis and basin modeling of the Matruh Basin, Western Desert, Egypt. Int. J. Geophys., https://doi.org/10.1155/2018/4931307.

Mukhopadhyay, P.K., 1994. Vitrinite reflectance as a maturity parameter. Petrographic and molecular characterization and its application to basin modeling. In: Mukhopadhyay, P.K., Dow, W.G. (Eds.), Vitrinite Reflectance as a Maturity Parameter. Applications and Limitations. Am. Chem. Soc. Symp. Series 570, pp. 1–24.

Mukhopadhyay, P.K., Gormly, J.R., Zumberge, J.E., 1989. Generation of hydrocarbons from the Tertiary coals of Texas: coal as potential source rock for liquid hydrocarbons in a deltaic basin. Org. Geochem. 14, 351–352.

Mutterlose, J., Harding, I.C., 1987. Phytoplankton from the anoxic sediments of the Barremian (lower Cretaceous) of north-west Germany. Abh. Geol. Bundesanst. (Vienna) 39, 177–215.

Norton, P., 1967. Rock-stratigraphic Nomenclatures of the Western Desert, Egypt. Unpublished Document. Pet. Corp., Egypt.

Pasley, M.A., 1991. Organic matter variation within depositional sequences stratigraphic significance of implication to petroleum source rock prediction. Unpublished PhD thesis, Louisiana University, USA, Pearson, D.L., 1990. Pollen/spore Color "standard". Phillips Pet. Co., Geol. Branch, Bartlesville, Oklahoma.

Pepper, A., S., Corvi, P., J., 1995. Simple kinetic models of petroleum formation. Part I: Oil and gas generation from kerogen. Mar. Pet. Geol. 12, 291-319.

Peters, K.E., Cassa, M.R., 1994. Applied source rock geochemistry. In: Magoon, L.B., Dow, W.G. (Eds.), The Petroleum System from Source to Trap. AAPG Mem., pp. 93–117.

Phipps D, Playford G. 1984. Laboratory techniques for extraction of palynomorphs from sediments. Papers Dept. Geol., Univ Queensland 11, 1–23.

Pickel, W., Kus, J., Flores, D., Kalaitzidis, S., Christanis, K., Cardott, B.J., Misz-Kennan, M., Rodrigues, S., Hentschel, A., Hamor-Vido, M., Crosdale, P., Wagner, N., ICCP, 2017. Classification of liptinite – ICCP System 1994. Int. J. Coal Geol. 169, 40–61.

Pocklington, R., Leonard, J.D., 1979. Terrigenous organic mattter in sediments of the St. Lawrence Estuary and the Saguenay Fjord. J. Fish. Res. Board Canada 36, 1250–1255.

Powell, T.G., Boreham, C.J., 1994. Terrestrially sourced oils: where do they exist and what are our limits of knowledge? In: Scott, A.C., Fleet, A.J. (Eds.), Coal and Coalbearing Strata as Oil-Prone Source Rocks. Geol. Soc. London Spec. Publ. 77, pp. 11–29.

Prauss, L.M., 2006. The Cenomanian/Turonian Boundary Event (CTBE) at Wunstorf, north-west Germany, as reflected by marine palynology. Cret. Res. 27, 872–886.

Shahin, A.N., 1992. Undiscovered petroleum reserves in northern Western Desert, Egypt. Proceed. 1st Int. Conf. Geol. Arab World, Cairo, Egypt, pp. 30–31.

Said, R., 1990. Cretaceous paleogeographic maps. In: Said, R. (Ed.), The Geology of Egypt. Balkema, Rotterdam, pp. 439–449.

Shalaby, M.R., Hakimi, M.H., Abdullah, W.H., 2011. Geochemical characteristics and hydrocarbon generation modeling of the Jurassic source rocks in the Shoushan Basin, north Western Desert, Egypt. Mar. Pet. Geol. 28, 1611–1624.

Shalaby, M.R., Hakimi, M.H., Abdullah, W.H., 2012. Organic geochemical characteristics and interpreted depositional environment of the Khatatba Formation, northern Western Desert, Egypt. AAPG Bull. 96, 2019–2036.

Singh, A., Shivanna, M., Mathews, R.P., Singh, B.D., Singh, H., Singh, V.P., Dutta, S., 2017a. Paleoenvironment of Eocene lignite bearing succession from Bikaner-Nagaur Basin, western India: Organic petrography, palynology, palynofacies and geochemistry. Int. J. Coal Geol. 181, 87–102.

Singh, V.P., Singh, B.D., Mathews, R.P., Singh, A., Mendhe, V.A., Singh, P.K., Mishra, S., Dutta, S., Shivanna, M., Singh, M.P., 2017b. Investigation on the lignite deposits of Surkha mine (Saurashtra Basin, Gujarat), western India: Their depositional history and hydrocarbon generation potential. Int. J. Coal Geol. 183, 78–99.

Stockmarr, J. 1971. Tablets with spores used in absolute pollen analysis. Pollen Spores 13, 616–621.

Suárez-Ruiz I., Flores, D., Mendonça Filho, J.G., Hackley, P.C., 2012. Review and update of the applications of organic petrology: Part 1, geological applications. Int. J. Coal Geol. 99, 54–112.

Sultan, N., Halim, A., 1988. Tectonic Framework of northern Western Desert, Egypt and its effect on hydrocarbon accumulations. Proceed. EGPC 9th Explor. Conf., Cairo, Egypt 2, 1–19.

Tahoun, S.S., Deaf, A.S., 2016. Could the conventionally known Abu Roash “G” reservoir (upper Cenomanian) be a promising active hydrocarbon source in the extreme northwestern part of Egypt? Palynofacies, palaeoenvironmental, and organic geochemical answers. Mar. Pet. Geol. 76, 231–245.

Tahoun, S.S., Deaf, A.S., Mansour, A., 2017. Palynological, palaeoenvironmental and sequence stratigraphical analyses of a Turonian-Coniacian sequence, Beni Suef Basin, Eastern Desert, Egypt: implication of Pediastrum rhythmic signature. Mar. Pet. Geol. 88, 871–887.

Tahoun, S.S., Deaf, A.S., Gentzis, T., Carvajal, H., 2017. Exceptional hydrocarbon source rock of the conventional (Albian) Kharita Formation reservoir in Matruh Basin, northern Western Desert of Egypt. AAPG Annual Convention and Exhibition, Houston, Texas, April 2–5, 2017. AAPG Data pages/Search and Discovery Article #90291.

Traverse, A., 1988. Paleopalynology. Unwin Hyman, Boston.

Traverse, A., 2007. Paleopalynology, 2nd ed. Springer, Dordrecht.

Tyson, R.V., 1995. Sedimentary Organic Matter: Organic Facies and Palynofacies. Chapman and Hall, London.

Tyson, R.V., 1996. Sequence-stratigraphical interpretation of organic facies variations in marine siliciclastic systems; general principles and application to the onshore Kimmeridge Clay Formation, UK. In: Hesselbo, S.P., Parkinson, D.N. (Eds.), Sequence Stratigraphy in British Geology, Geol. Soc. Spec. Publ., vol. 103, pp. 75–96.

Vallejo, C., Hochuli, P.A., Winkler, W., von Salis, K., 2002. Palynological and sequence stratigraphic analysis of the Napo Group in the Pungarayacu 30 well, Sub-Andean Zone, Ecuador. Cret. Res. 23, 845–859.

WEPCO, 1968. Final report and composite log of the Abu Tunis 1X well. Cairo.

WEPCO, 1970. Final report and composite log of the Siqeifa 1X well. Cairo.

Figure 1

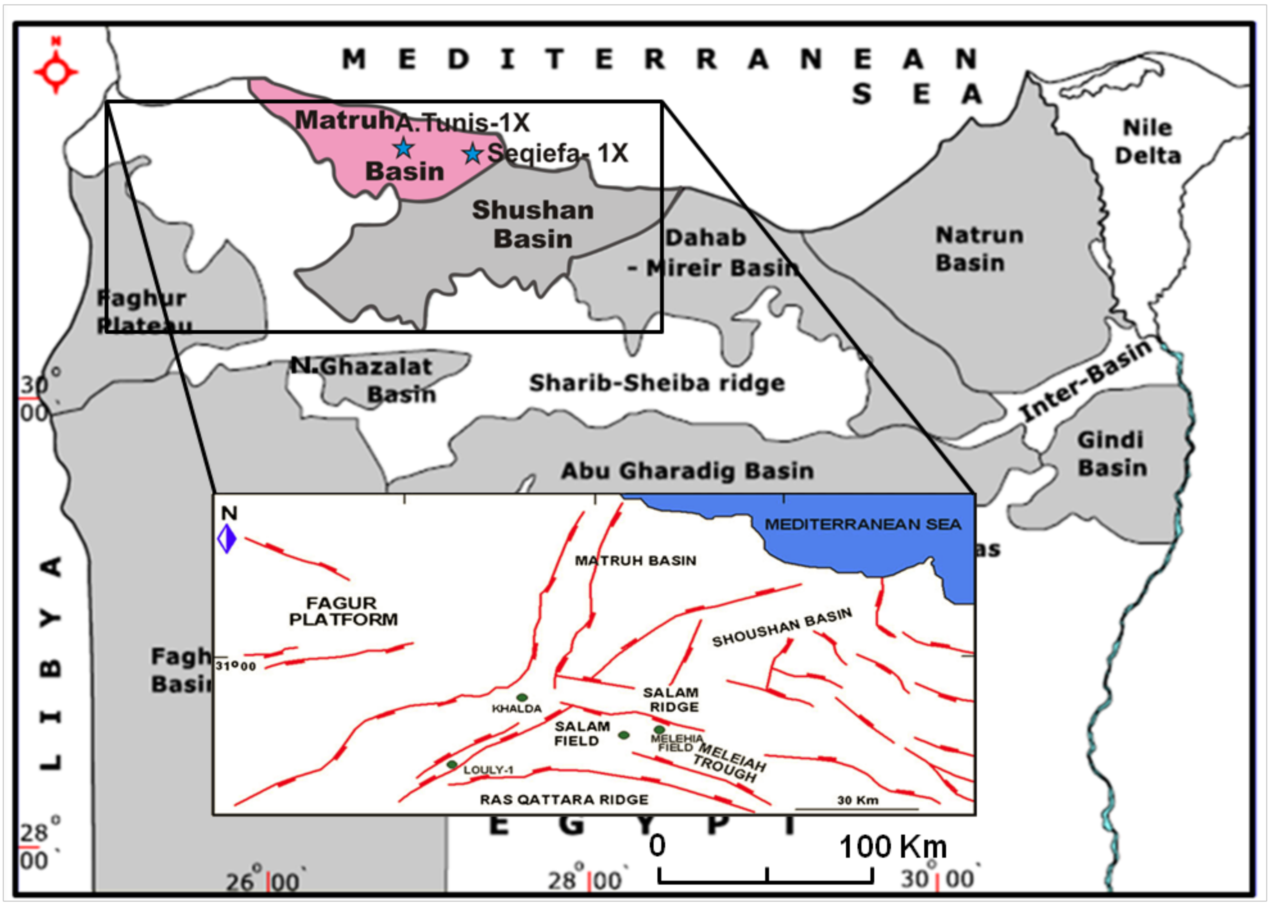
MEDITERRANEAN SEA
Matruh Basin
A.Tunis-1X
Seqiefa- 1X
Shushan Basin
Dahab - Mireir Basin
Natrun Basin
Nile Delta
Faghur Plateau
N.Ghazalat Basin
Sharib-Sheiba ridge
Inter-Basin
Gindi Basin
Abu Gharadig Basin
LIBYA
EGYPT
Faghur Basin
30° 00'
28° 00'
26° 00'
28° 00'
30° 00'
0
100 Km
N
MEDITERRANEAN SEA
MATRUH BASIN
FAGUR PLATFORM
SHOUSHAN BASIN
31°00
KHALDA
SALAM RIDGE
SALAM FIELD
MELEHIA FIELD
MELEIAH TROUGH
LOULY-1
RAS QATTARA RIDGE
30 Km

Figure 2

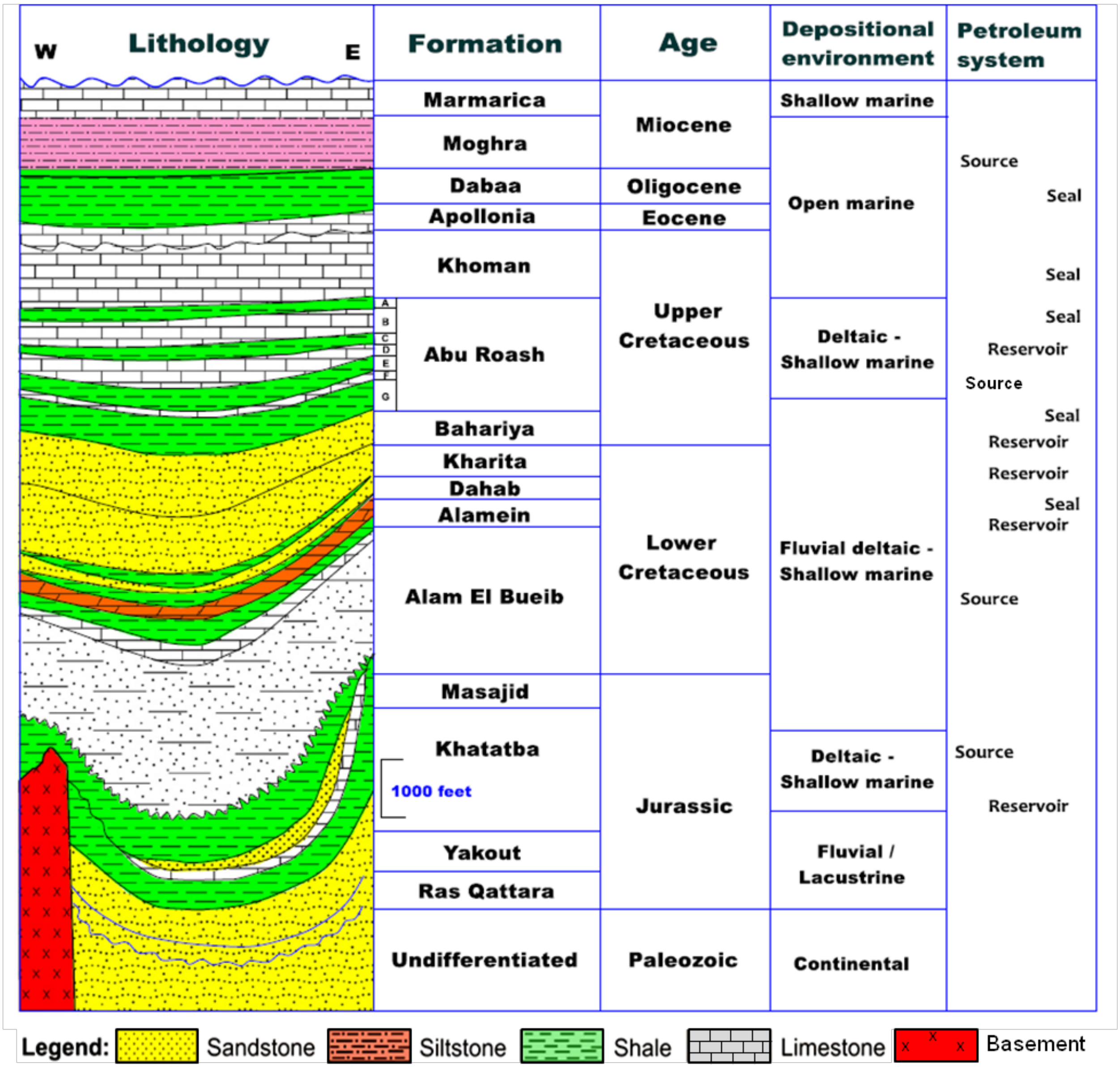

W
Lithology
E
Formation
Age
Depositional environment
Petroleum system
Marmarica
Moghra
Dabaa
Apollonia
Khoman
Abu Roash
A
B
C
D
E
F
G
Bahariya
Kharita
Dahab
Alamein
Alam El Bueib
Masajid
Khatatba
1000 feet
Yakout
Ras Qattara
Undifferentiated
Miocene
Oligocene
Eocene
Upper Cretaceous
Lower Cretaceous
Jurassic
Paleozoic
Shallow marine
Open marine
Deltaic - Shallow marine
Fluvial deltaic - Shallow marine
Deltaic - Shallow marine
Fluvial / Lacustrine
Continental
Source
Seal
Seal
Seal
Reservoir
Source
Seal
Reservoir
Reservoir
Seal
Reservoir
Source
Source
Reservoir
Legend:
Sandstone
Siltstone
Shale
Limestone
Basement

1229 **Figure 3**

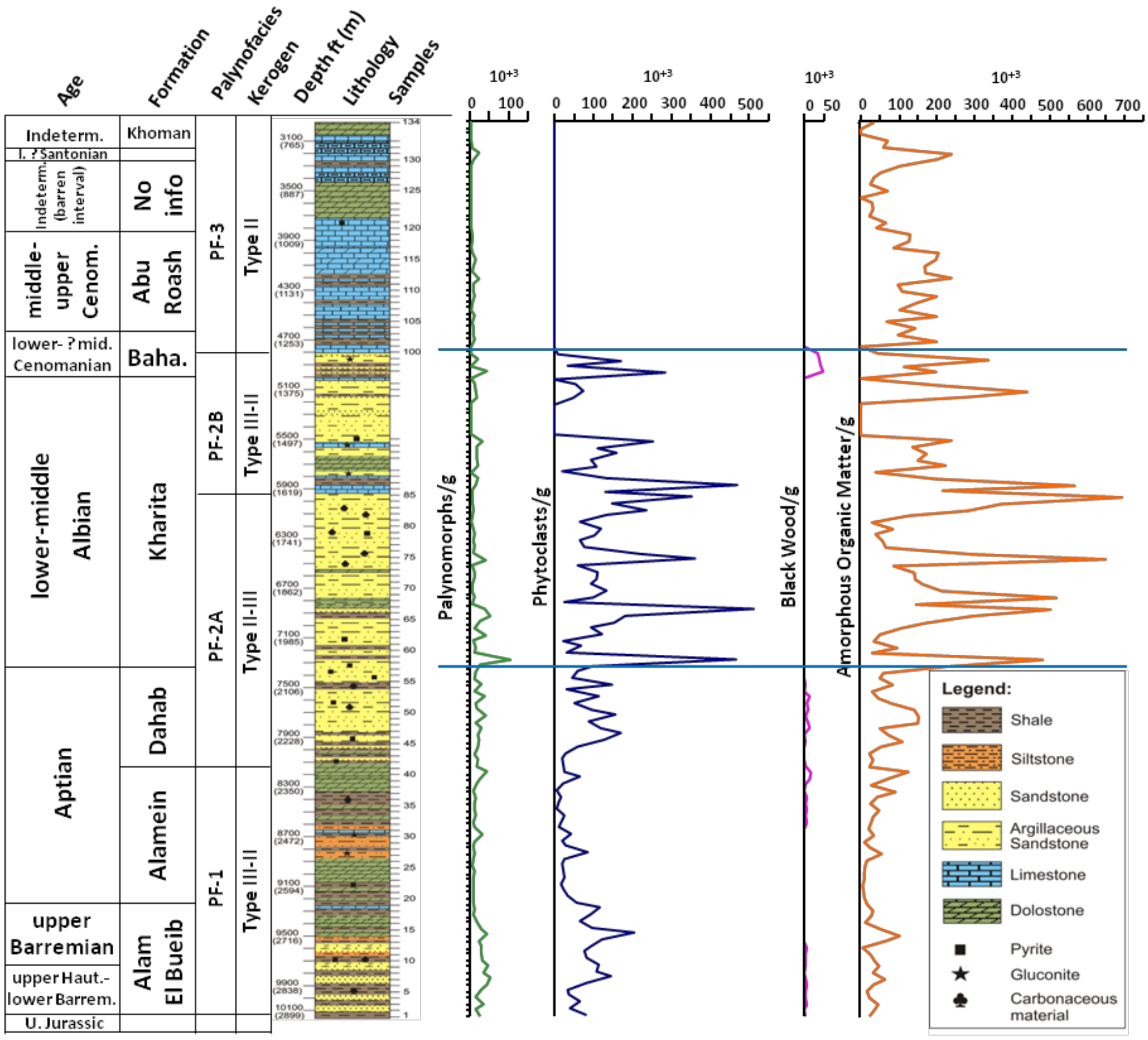

Figure 4

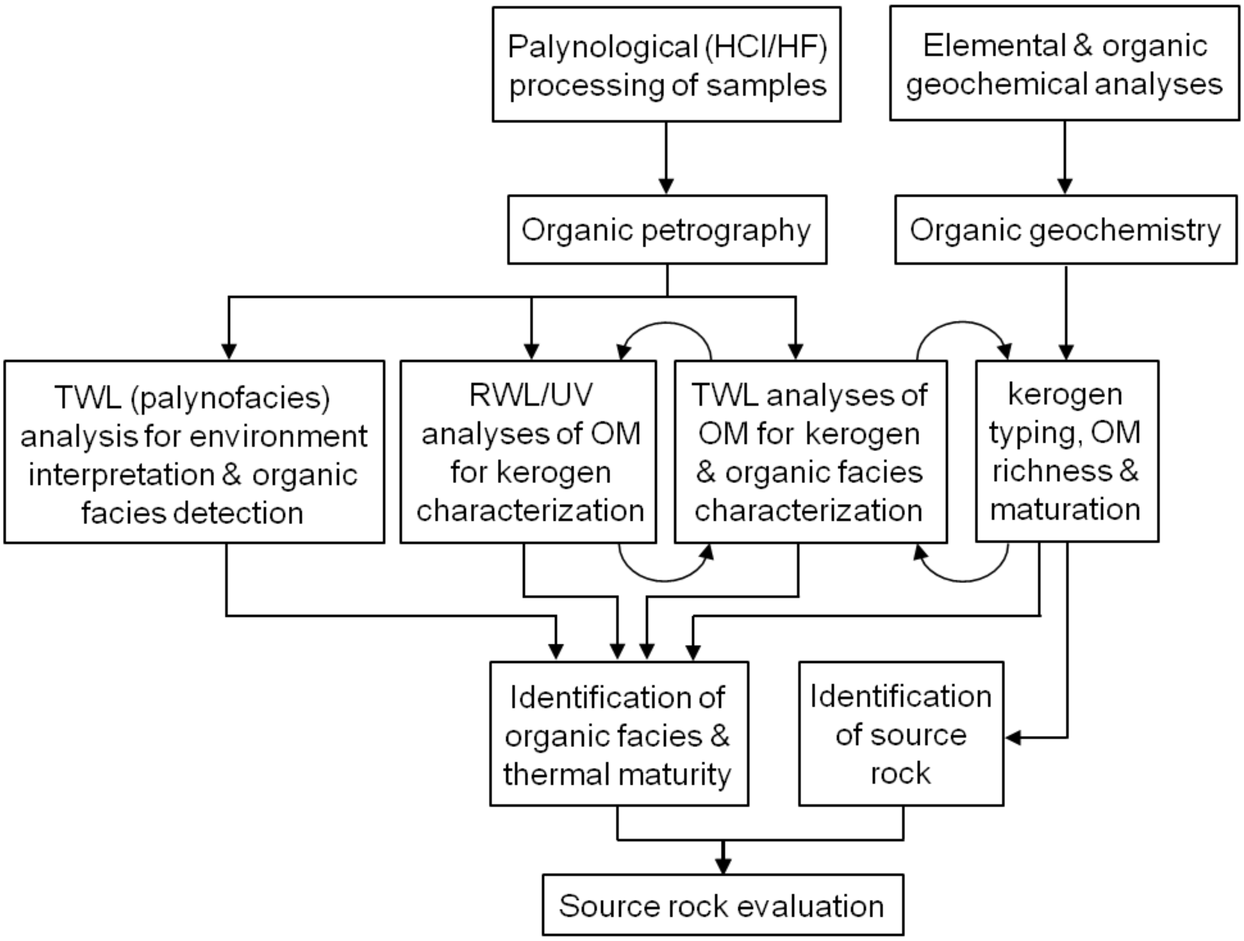
Palynological (HCl/HF) processing of samples
Elemental & organic geochemical analyses
Organic petrography
Organic geochemistry
TWL (palynofacies) analysis for environment interpretation & organic facies detection
RWL/UV analyses of OM for kerogen characterization
TWL analyses of OM for kerogen & organic facies characterization
kerogen typing, OM richness & maturation
Identification of organic facies & thermal maturity
Identification of source rock
Source rock evaluation

1231 **Figure 5**

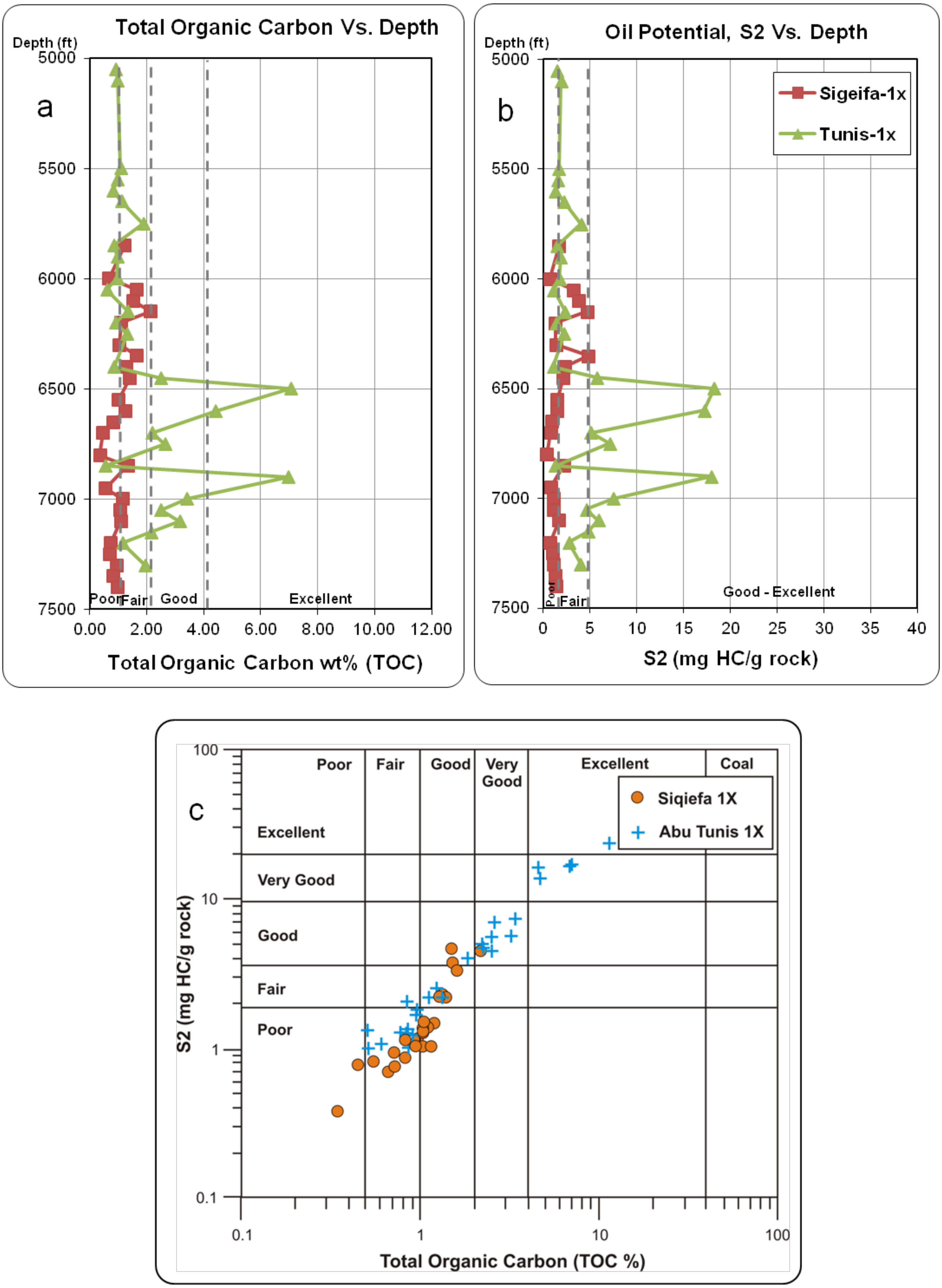

1232 **Figure 6**

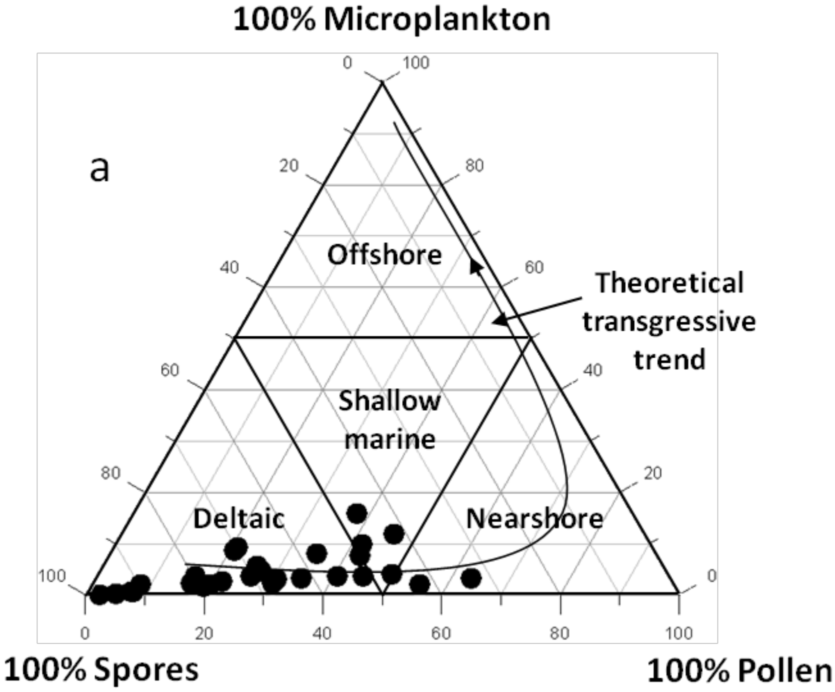

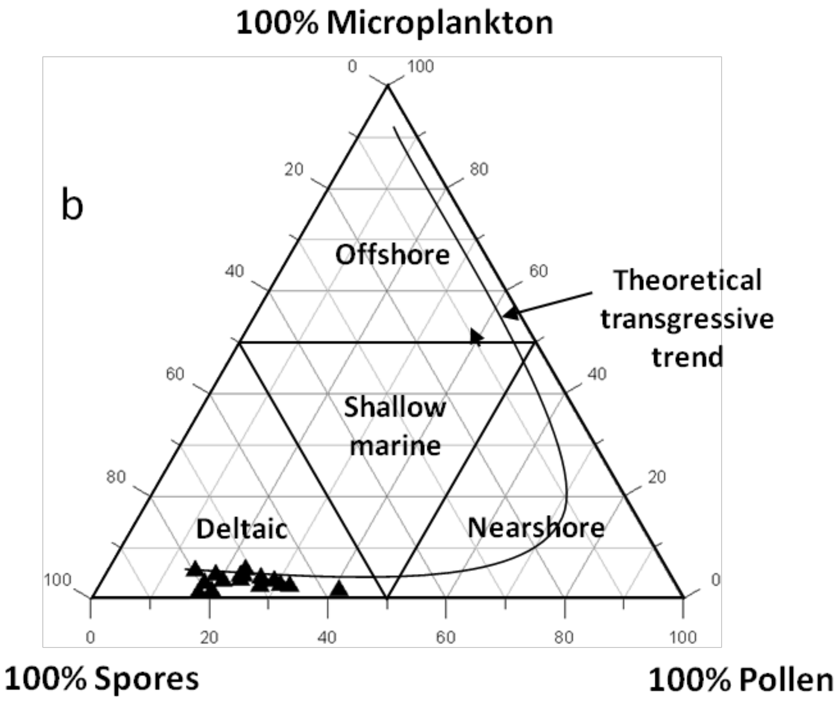

1233 **Figure 7**

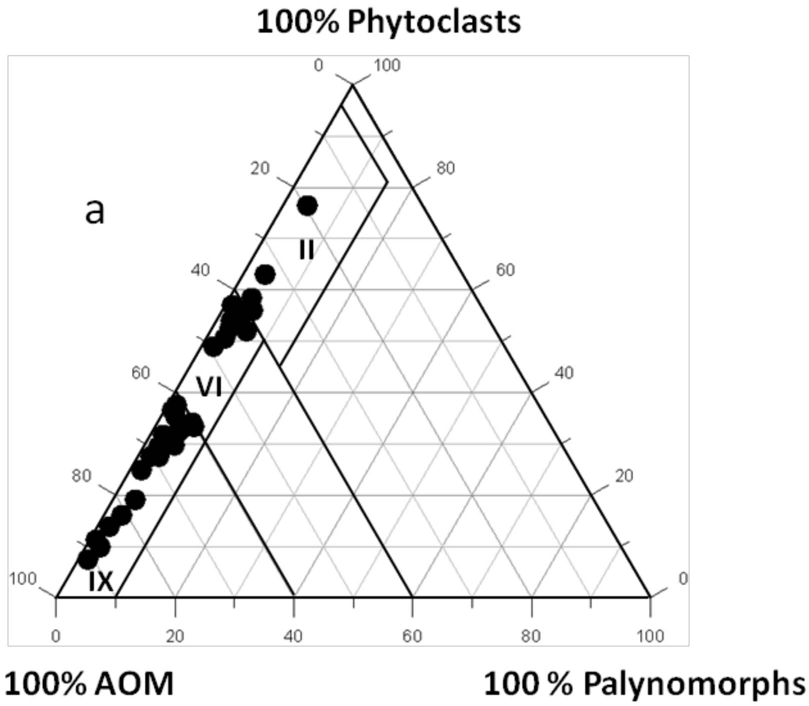

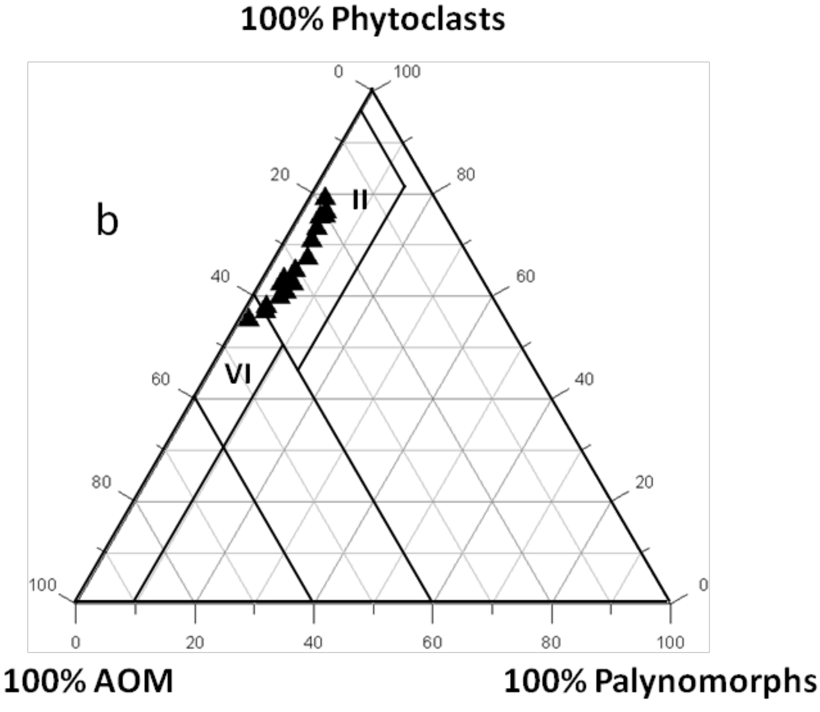

1234 **Figure 8**

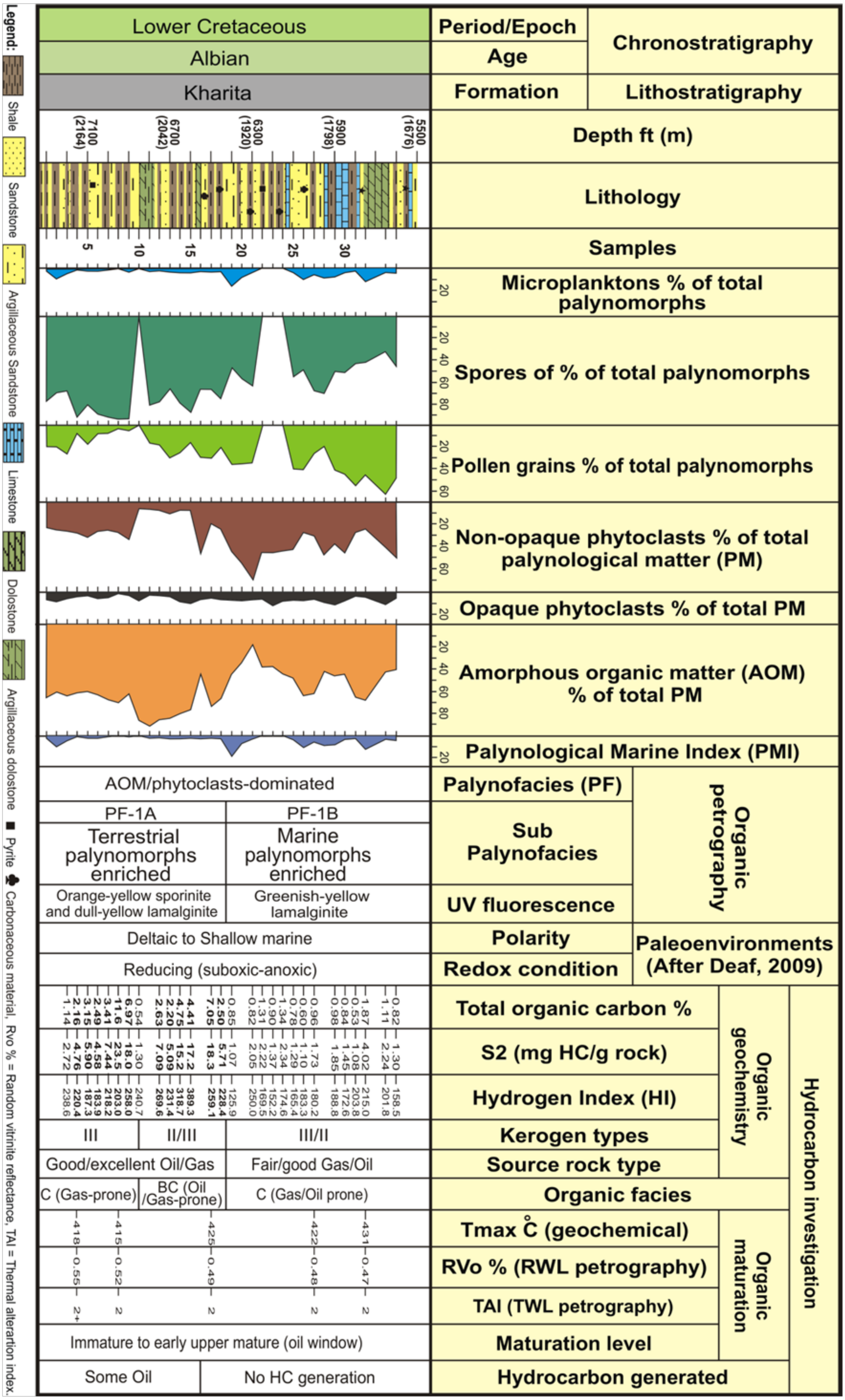

Figure 9

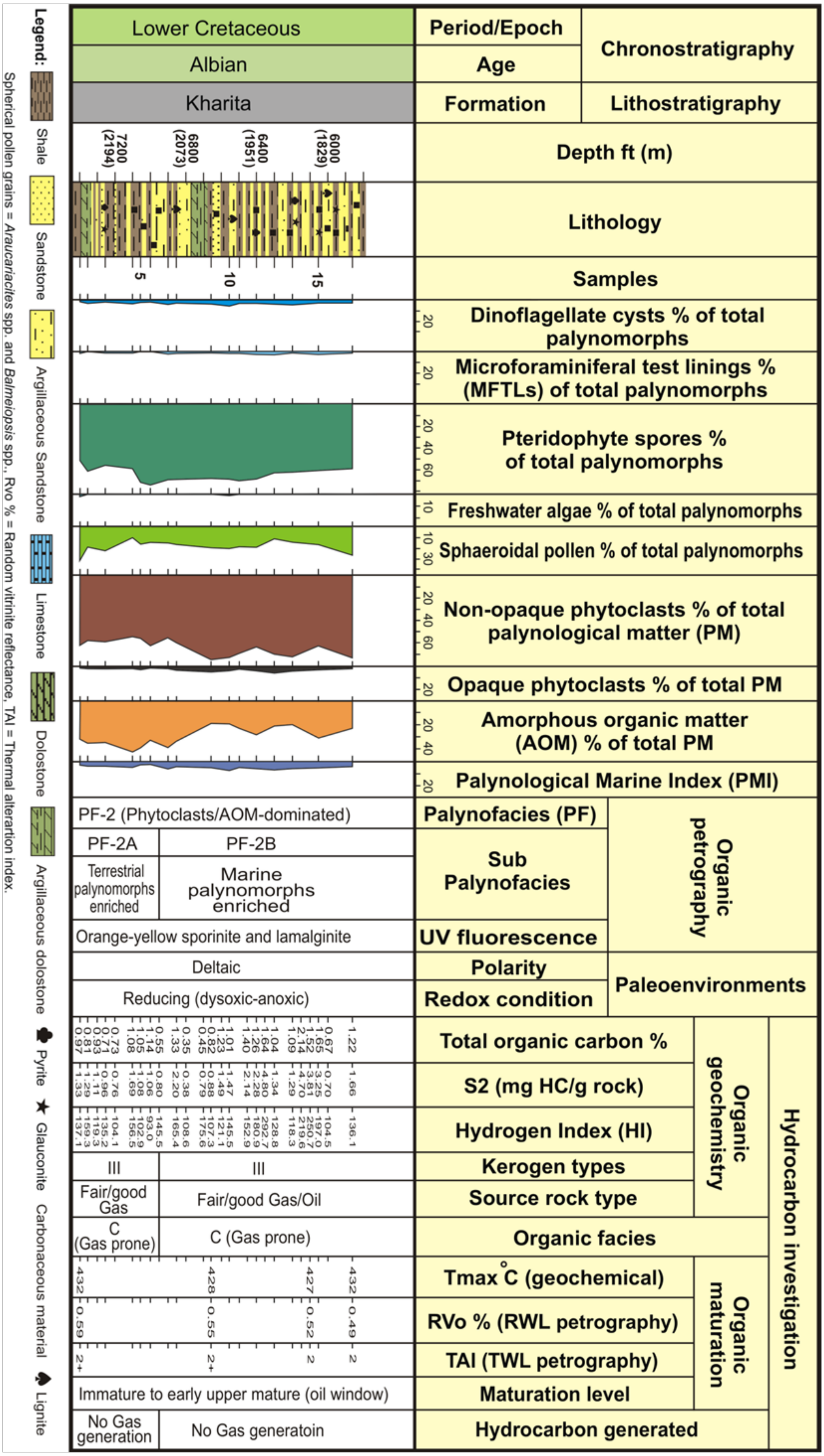

Lower Cretaceous
Albian
Kharita
Period/Epoch
Age
Chronostratigraphy
Formation
Lithostratigraphy
6000 (1829)
6400 (1951)
6800 (2073)
7200 (2194)
Depth ft (m)
Lithology
Samples
Dinoflagellate cysts % of total palynomorphs
Microforaminiferal test linings % (MFTLs) of total palynomorphs
Pteridophyte spores % of total palynomorphs
Freshwater algae % of total palynomorphs
Sphaeroidal pollen % of total palynomorphs
Non-opaque phytoclasts % of total palynological matter (PM)
Opaque phytoclasts % of total PM
Amorphous organic matter (AOM) % of total PM
Palynological Marine Index (PMI)
PF-2 (Phytoclasts/AOM-dominated)
Palynofacies (PF)
PF-2A
PF-2B
Terrestrial palynomorphs enriched
Marine palynomorphs enriched
Sub Palynofacies
Organic petrography
Orange-yellow sporinite and lamalginite
UV fluorescence
Deltaic
Polarity
Reducing (dysoxic-anoxic)
Redox condition
Paleoenvironments
Total organic carbon %
S2 (mg HC/g rock)
Hydrogen Index (HI)
III
III
Kerogen types
Fair/good Gas
Fair/good Gas/Oil
Source rock type
Organic geochemistry
C (Gas prone)
C (Gas prone)
Organic facies
Tmax °C (geochemical)
RVo % (RWL petrography)
TAI (TWL petrography)
Immature to early upper mature (oil window)
Maturation level
Organic maturation
No Gas generation
No Gas generatoin
Hydrocarbon generated
Hydrocarbon investigation
Legend:
Shale
Sandstone
Argillaceous Sandstone
Limestone
Dolostone
Argillaceous dolostone
Pyrite
Glauconite
Carbonaceous material
Lignite
Spherical pollen grains = Araucariacites spp. and Balmeiopsis spp., Rvo % = Random vitrinite reflectance, TAI = Thermal alteration index.

1236 **Figure 10**

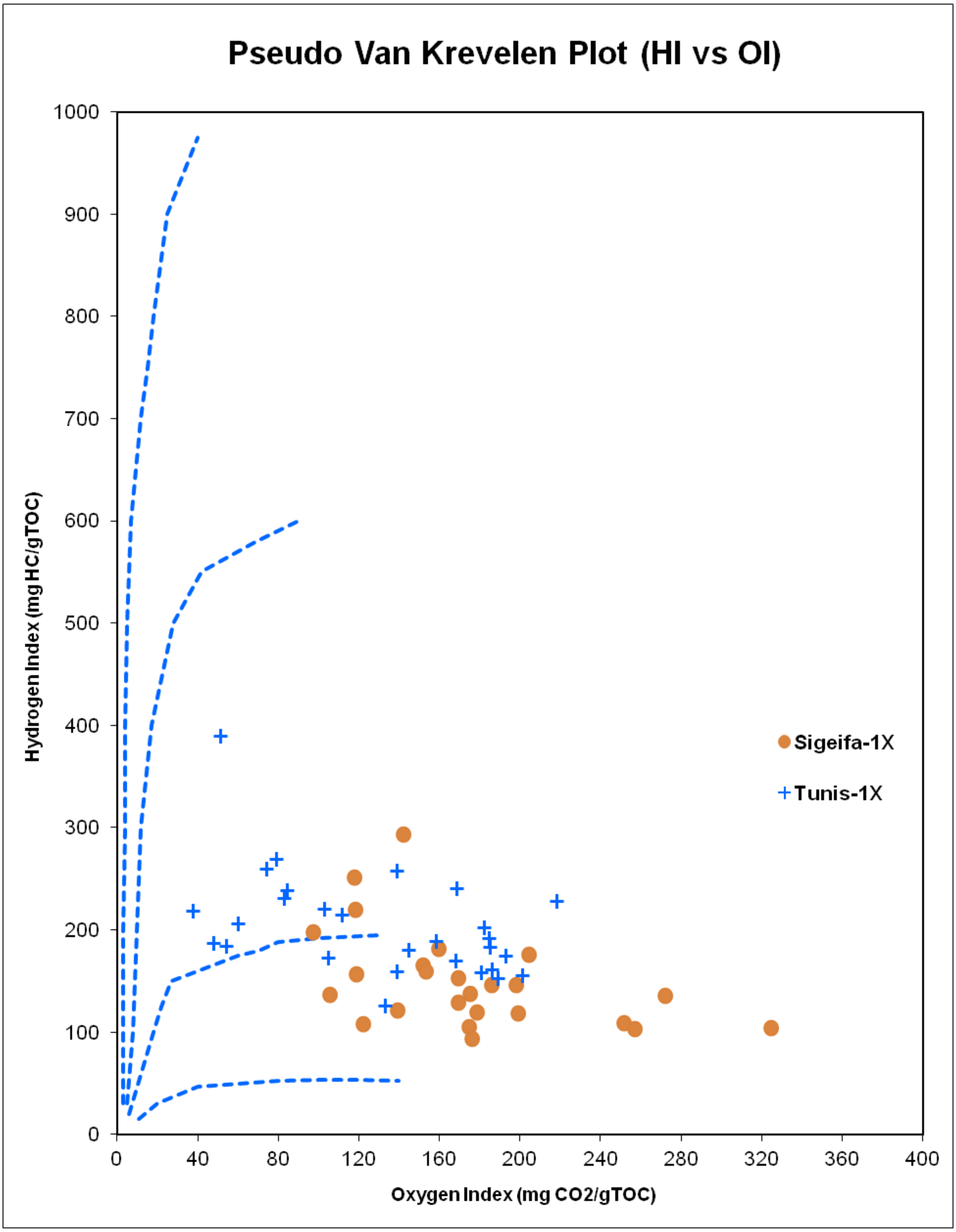

1237 **Figure 11**

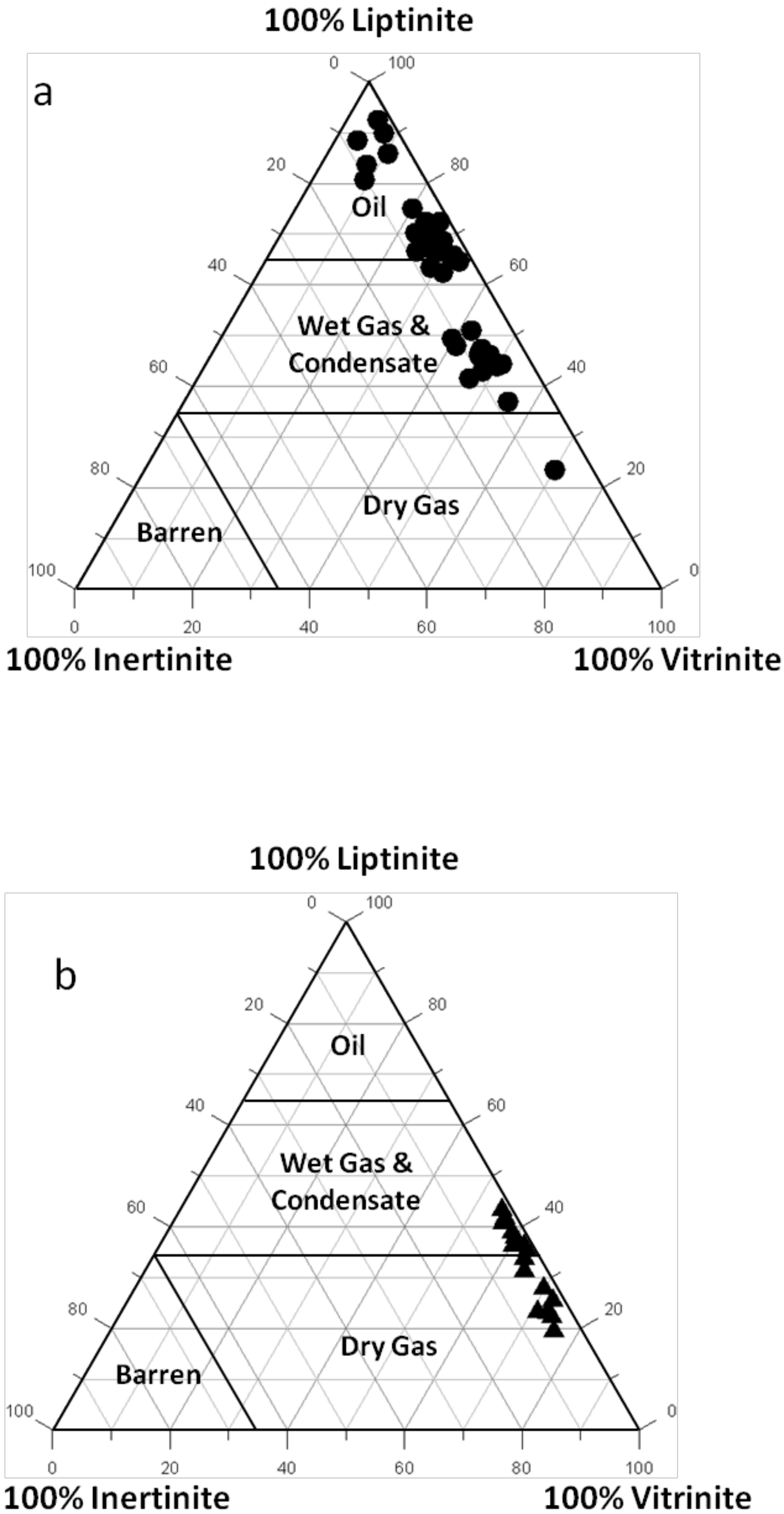

Figure 12

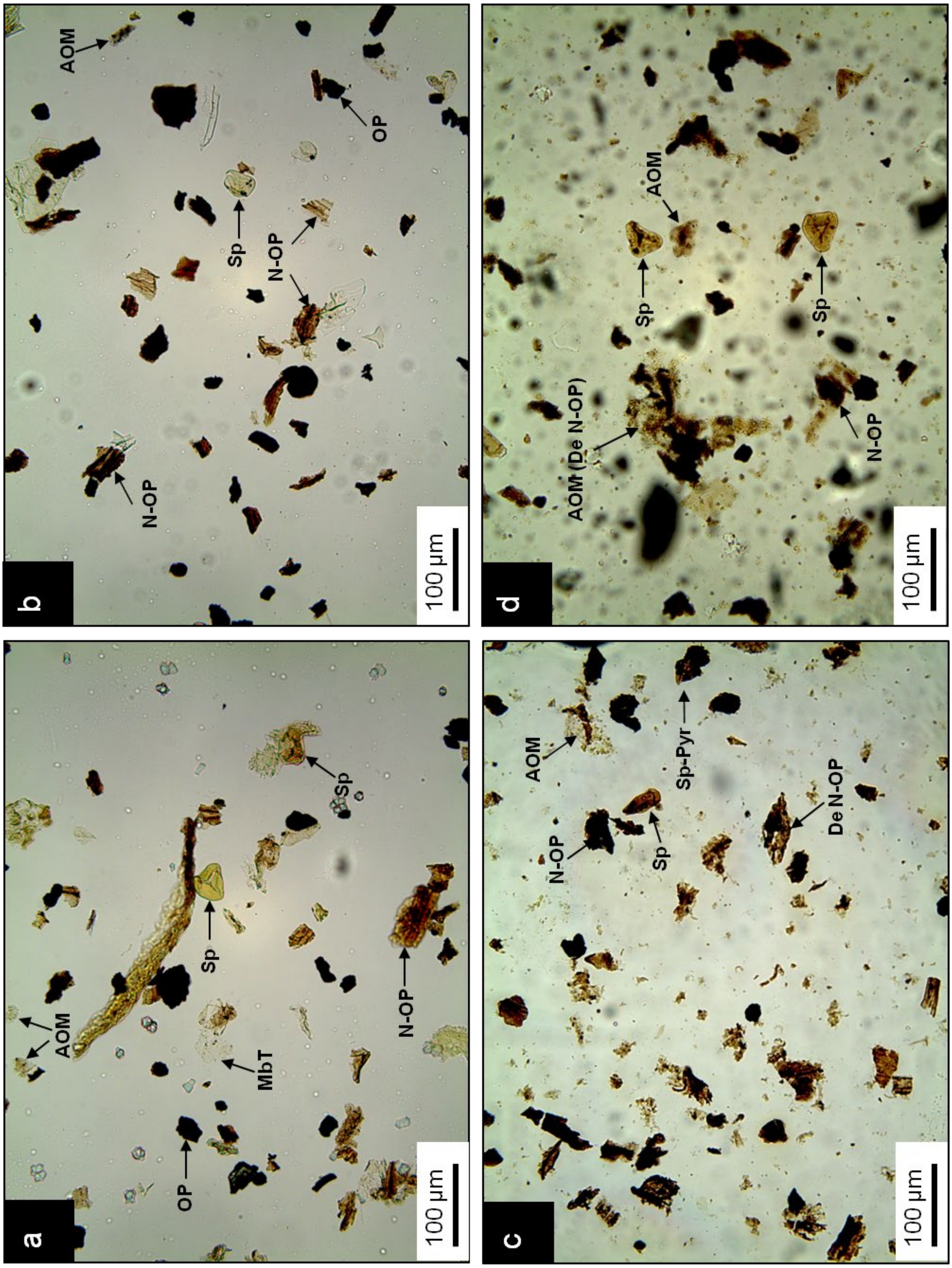
a
AOM
Sp
MbT
OP
N-OP
100 µm
b
AOM
OP
Sp
N-OP
N-OP
100 µm
c
AOM
N-OP
Sp
Sp-Pyr
De N-OP
100 µm
d
AOM
Sp
AOM (De N-OP)
Sp
N-OP
100 µm

1239 **Figure 13**

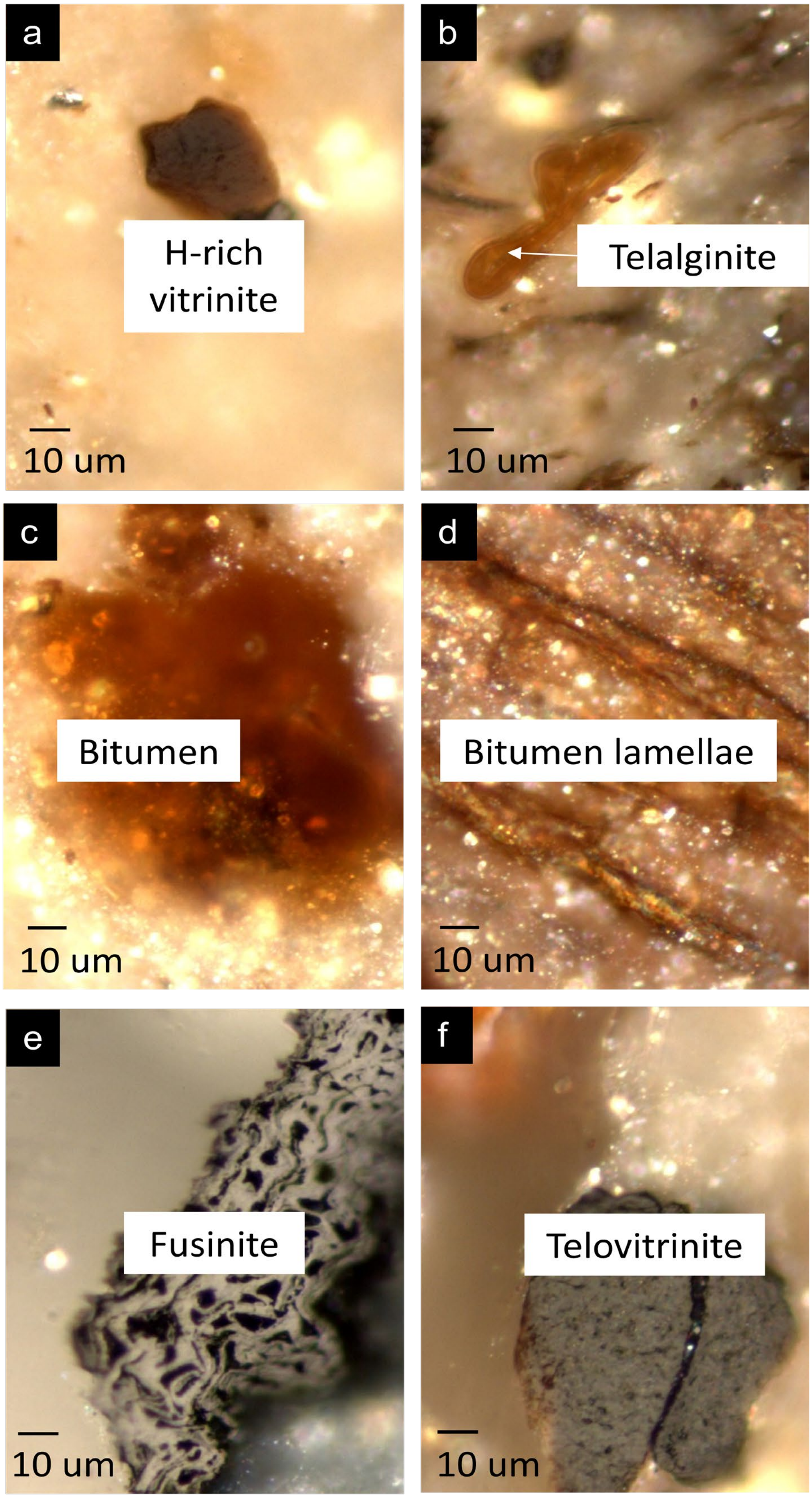

1240 **Figure 14**

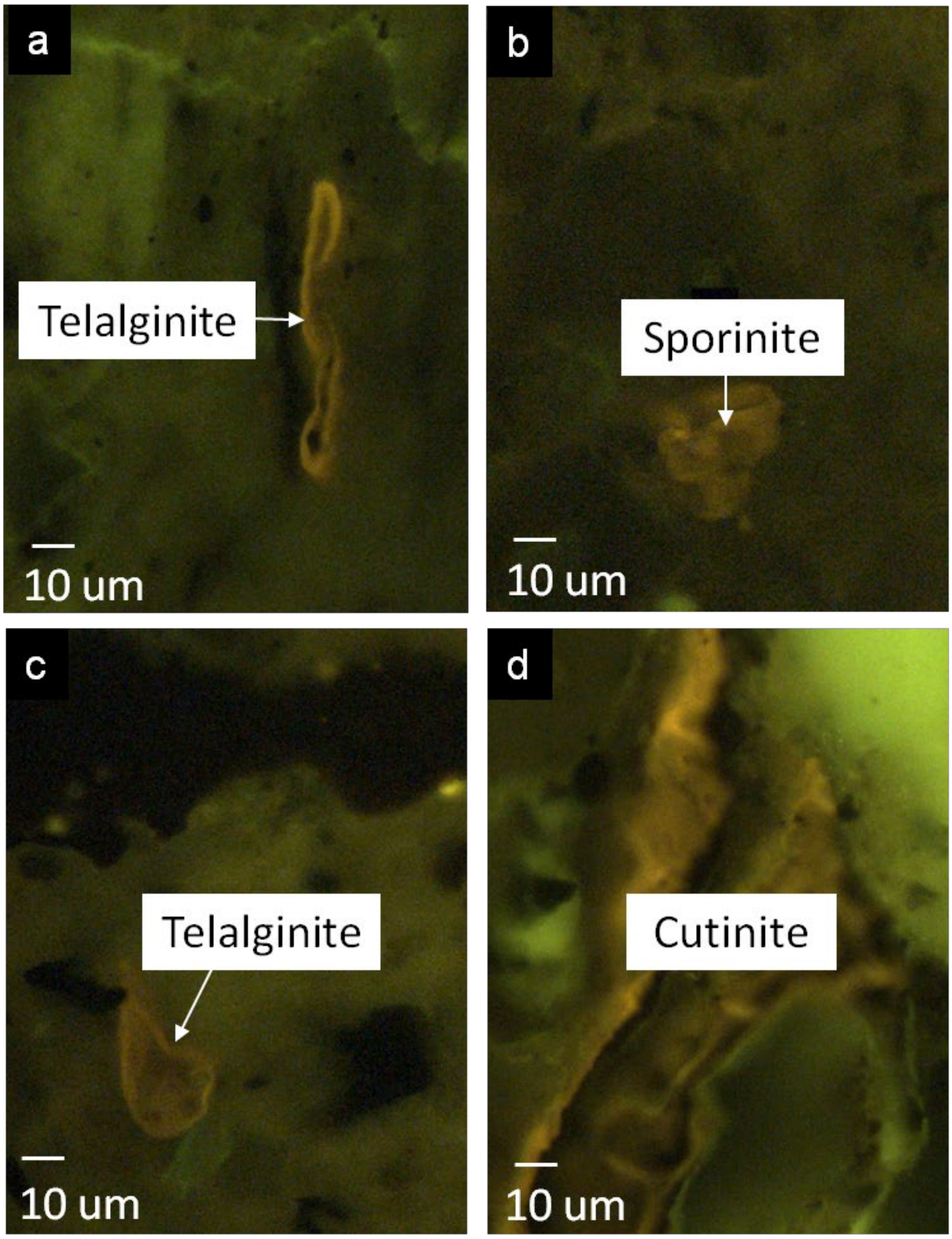

1241 **Figure 15**

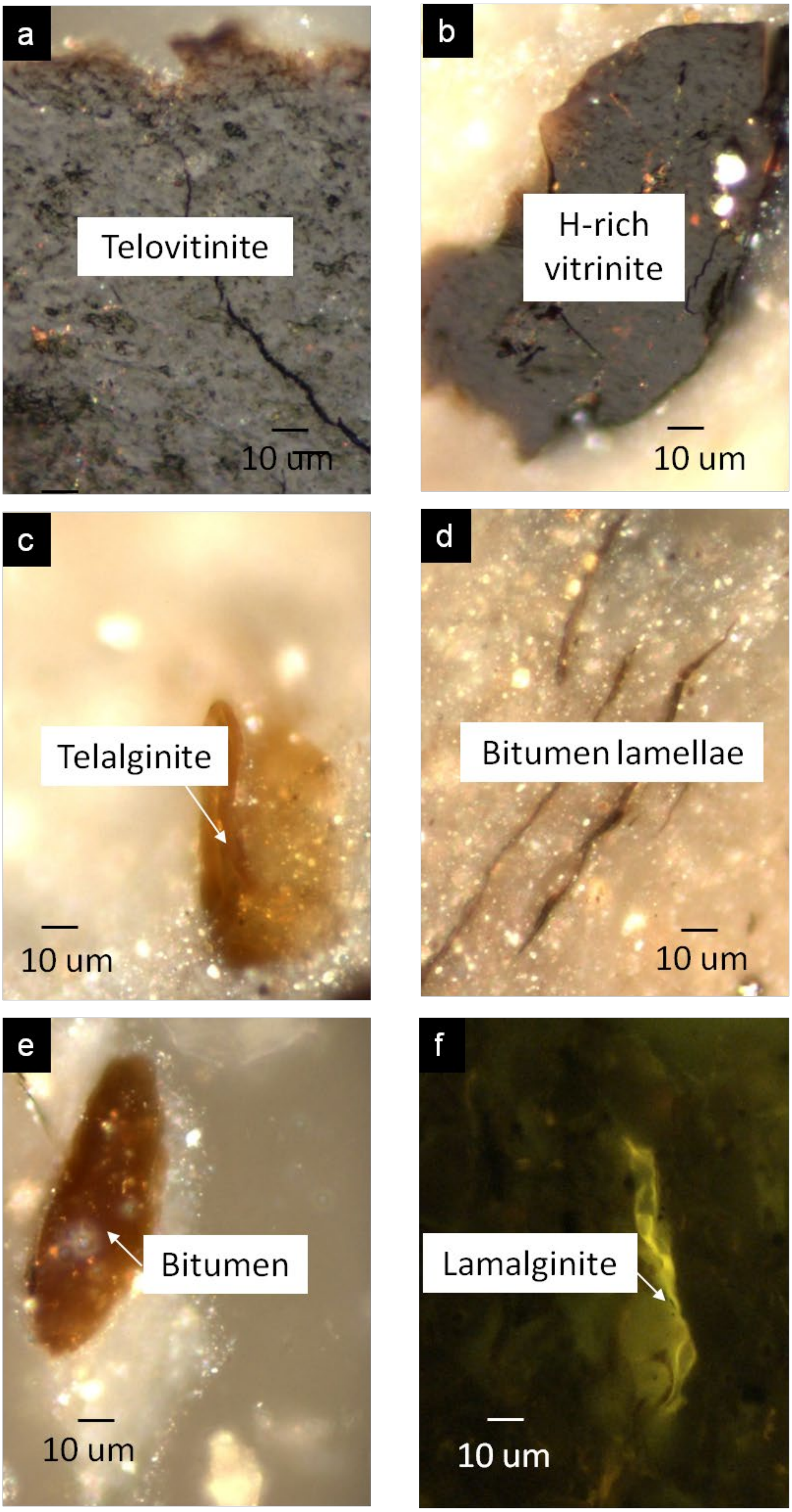

1242 **Figure 16**

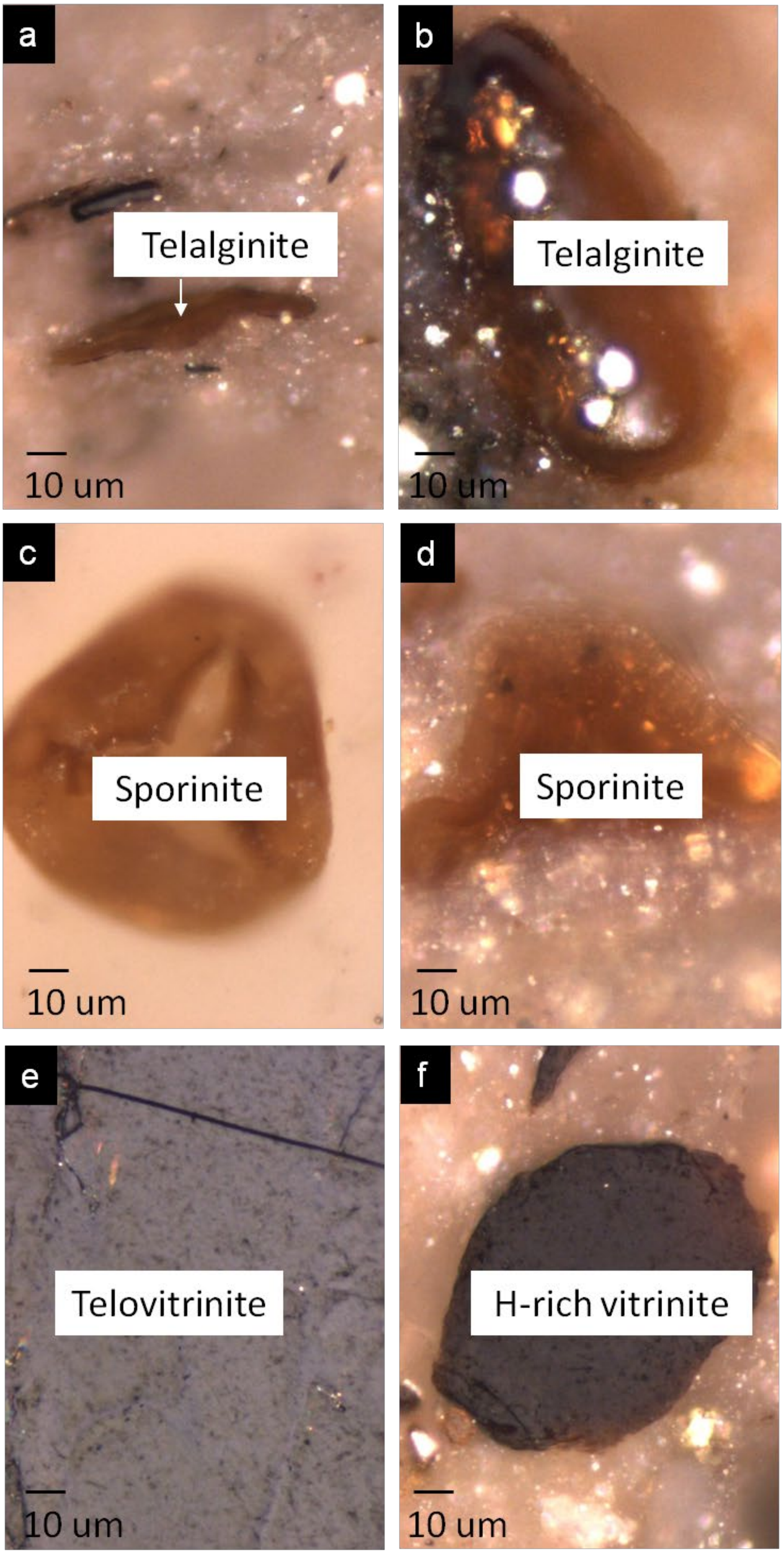

1243 **Figure 17**

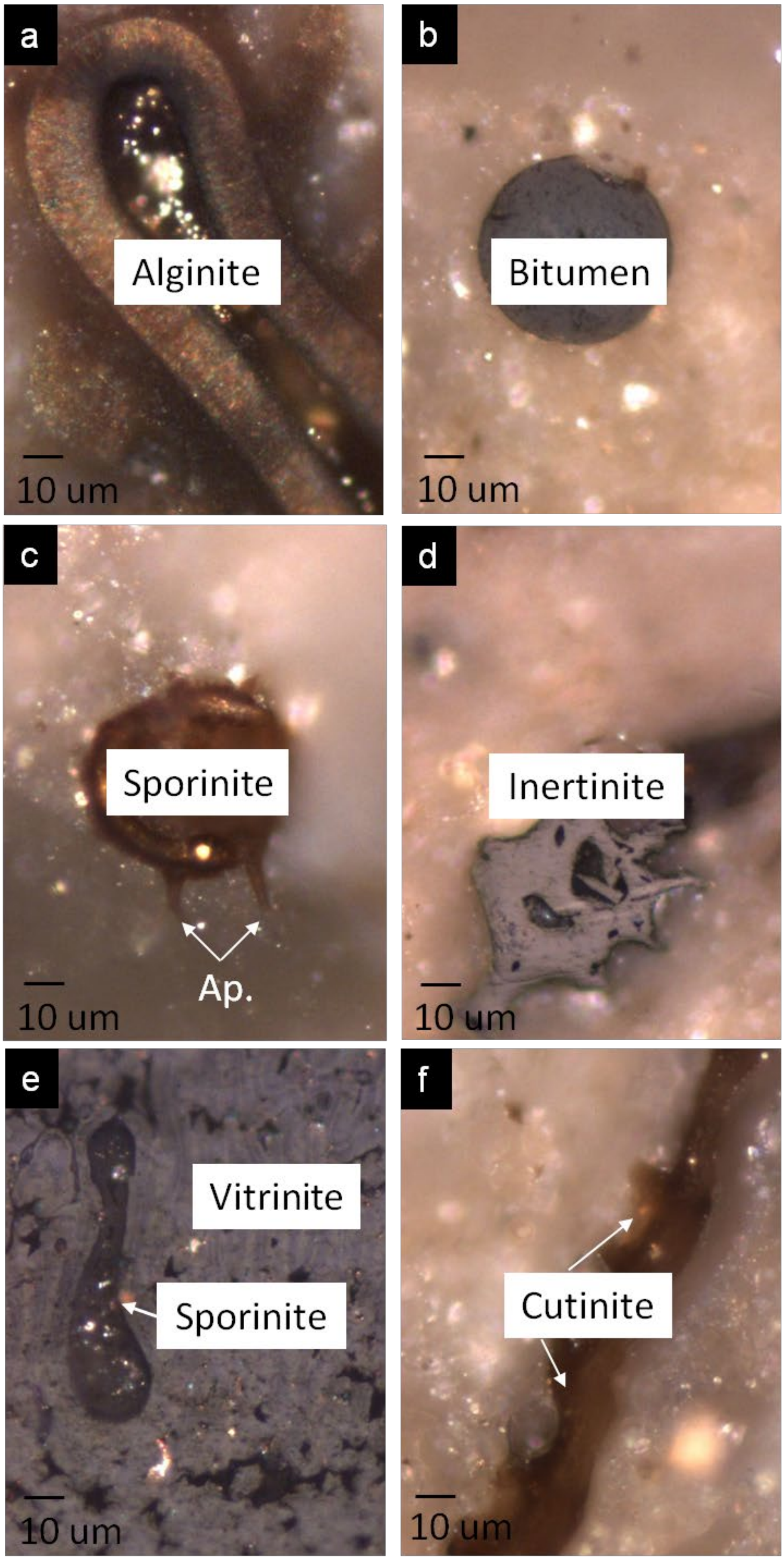

1244 **Figure 18**

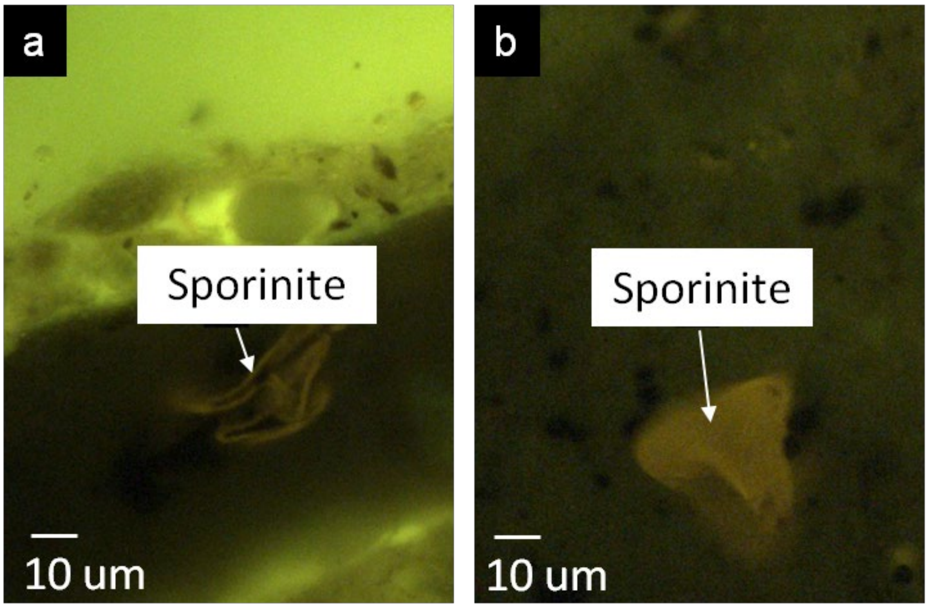

1245 **Figure 19**

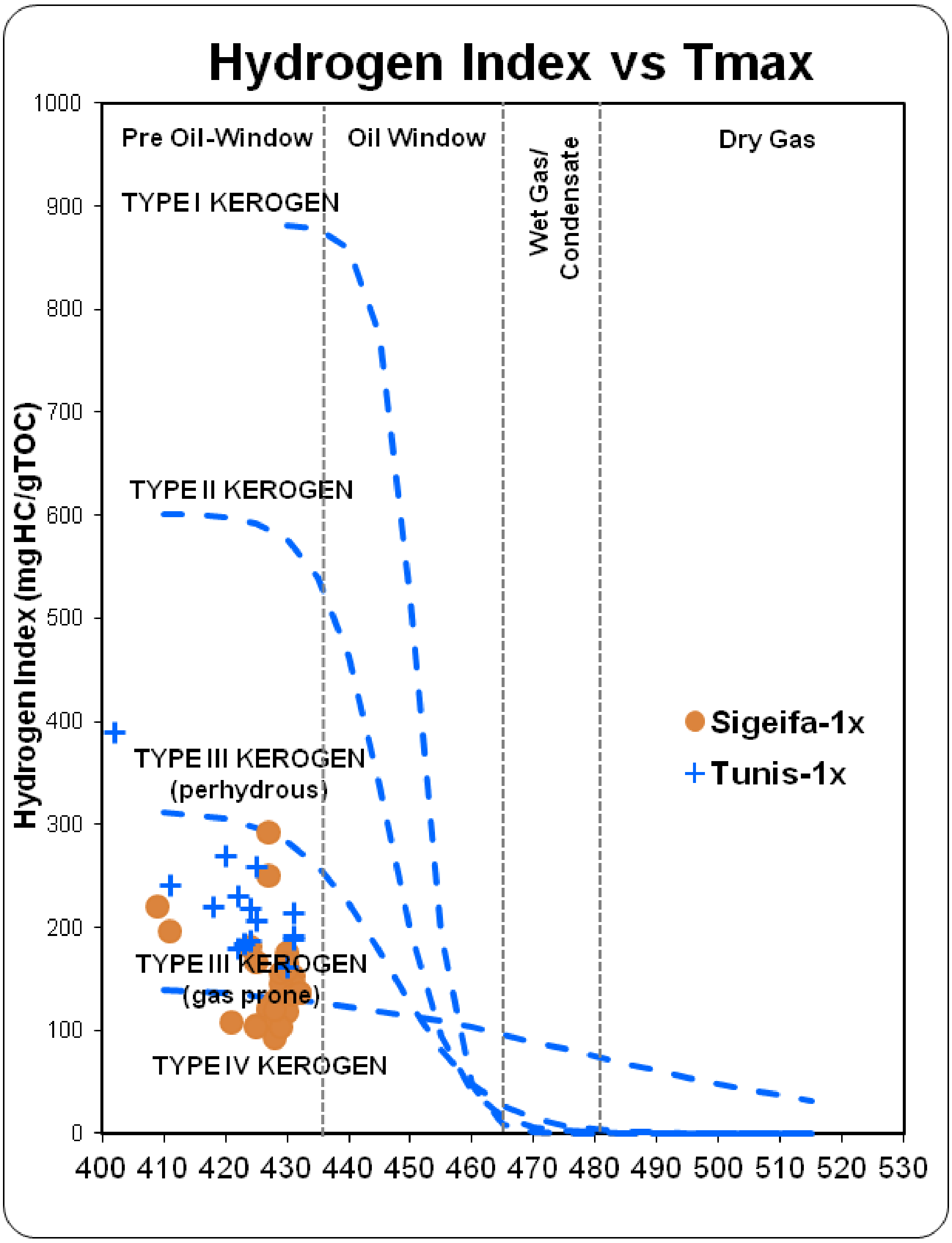

Figure 20

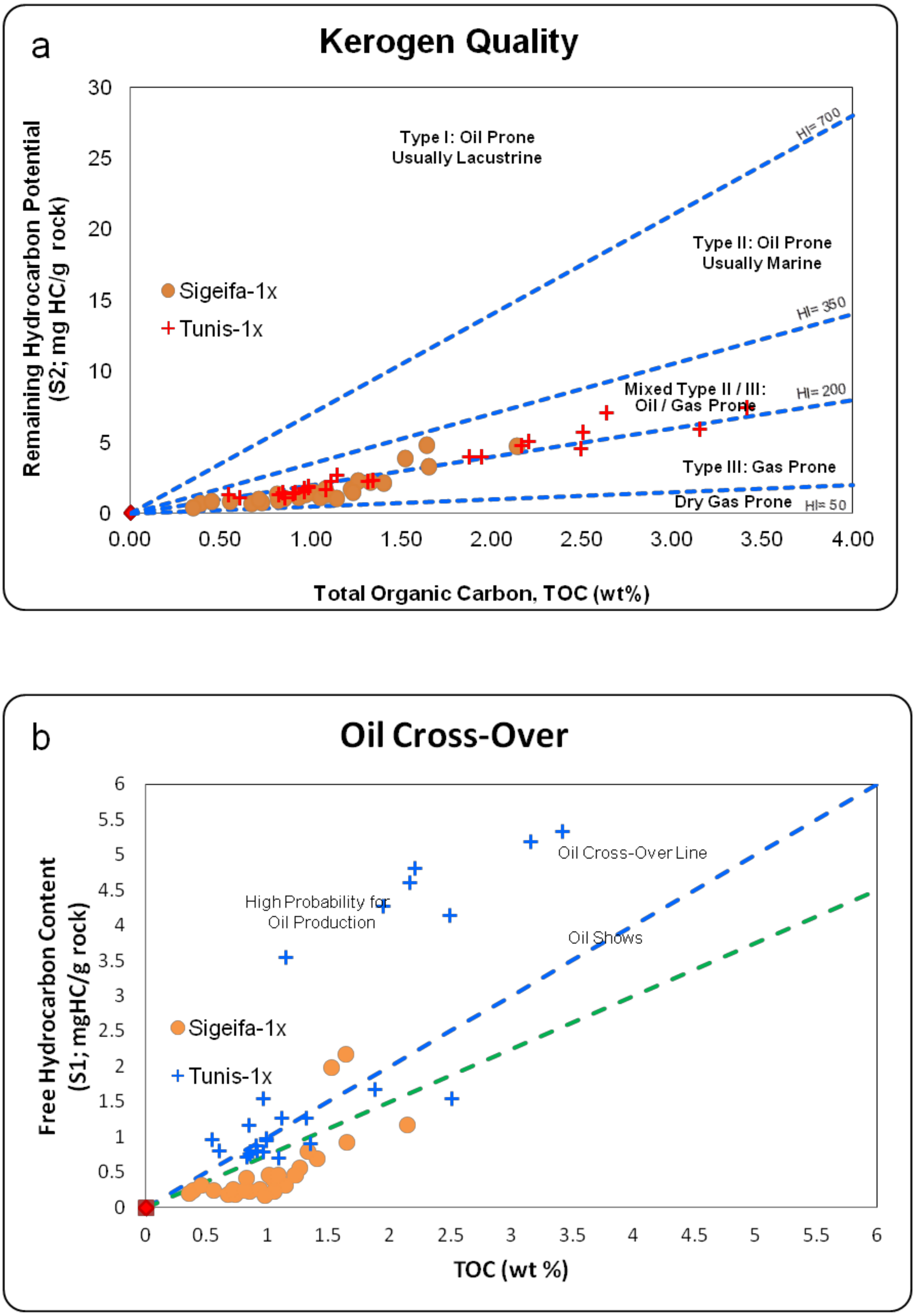
a
Kerogen Quality
Remaining Hydrocarbon Potential
(S2; mg HC/g rock)
Total Organic Carbon, TOC (wt%)
Type I: Oil Prone
Usually Lacustrine
Type II: Oil Prone
Usually Marine
Mixed Type II / III:
Oil / Gas Prone
Type III: Gas Prone
Dry Gas Prone
HI= 700
HI= 350
HI= 200
HI= 50
Sigeifa-1x
Tunis-1x
0
5
10
15
20
25
30
0.00
0.50
1.00
1.50
2.00
2.50
3.00
3.50
4.00
b
Oil Cross-Over
Free Hydrocarbon Content
(S1; mgHC/g rock)
TOC (wt %)
High Probability for
Oil Production
Oil Cross-Over Line
Oil Shows
Sigeifa-1x
Tunis-1x
0
0.5
1
1.5
2
2.5
3
3.5
4
4.5
5
5.5
6

Figure 21

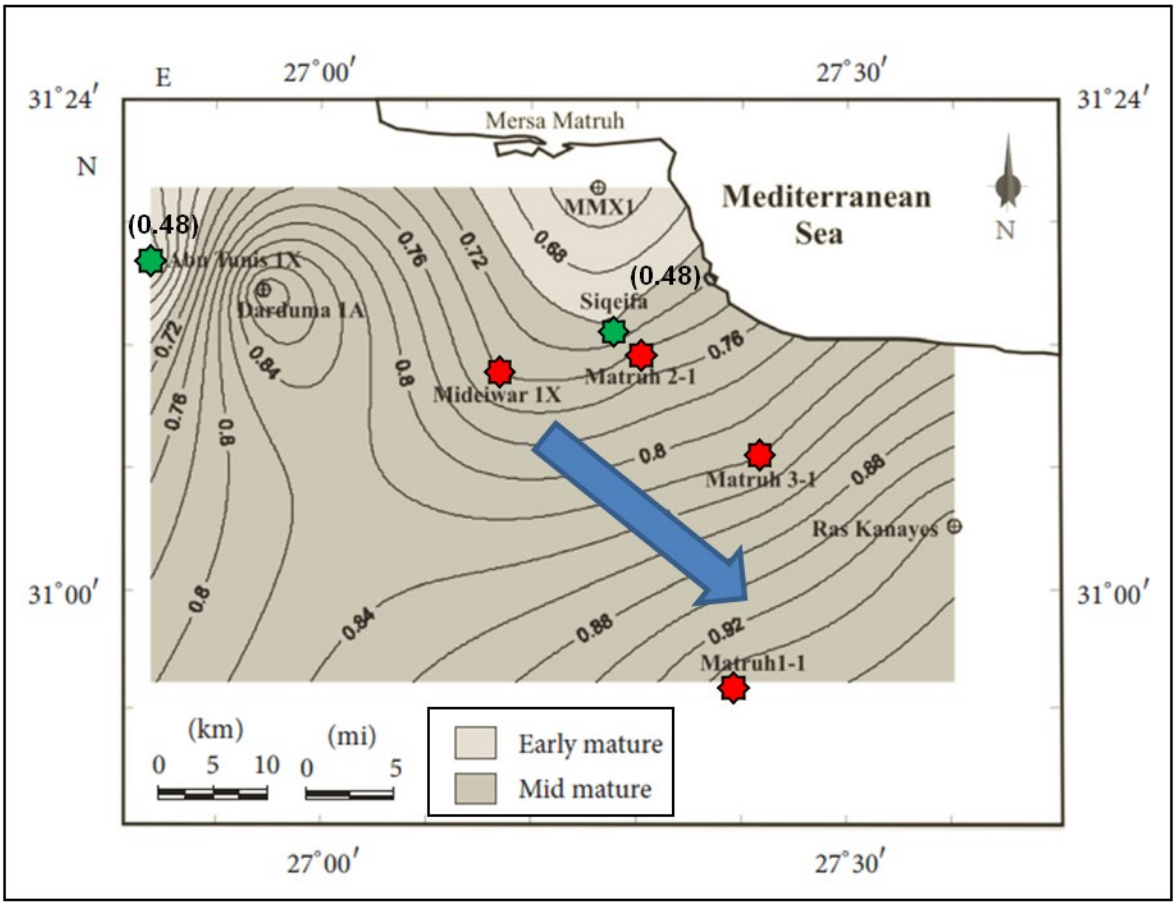

27°00′
27°30′
31°24′
E
N
Mersa Matruh
MMX1
Mediterranean
Sea
N
(0.48)
Darduma 1A
(0.48)
Siqeifa
Matruh 2-1
Mideiwar 1X
Matruh 3-1
Ras Kanayes
Matruh1-1
0.72
0.76
0.8
0.84
0.68
0.88
0.92
31°00′
(km)
0 5 10
(mi)
0 5
Early mature
Mid mature

Table 1

Samples No.	Depth ft	Depth m	TOC wt %	S1 mg HC/g rock	S2 mg HC/g rock	S3 mg CO2/g rock	S3 mg CO/g rock	HI mg HC/g TOC	OI mg HC/g TOC	PI mg HC/g rock	OSI mg HC/g TOC	Oil in Rock bbl oil/ac-ft	Tmax °C	VRo (%)
28	5600	1706.9	0.82	0.72	1.3	1.48	0.28	158.54	180.49	0.36	87.80	15.76	298	0.46
27	5650	1722.1	**1.11**	1.27	**2.24**	2.02	0.43	201.80	181.98	0.36	114.41	27.80	309	0.47
26	5750	1752.6	**1.87**	1.69	4.02	2.08	0.74	214.97	111.23	0.30	90.37	36.99	431	0.47
25	5800	1767.8	0.53	0.77	1.08	0.81	0.22	203.77	152.83	0.42	145.28	16.86	428	
24	5850	1783.1	0.84	1.18	1.45	0.88	0.11	172.62	104.76	0.45	140.48	25.83	292	0.47
23	5900	1798.3	0.98	0.98	1.85	1.55	0.41	188.78	158.16	0.35	100.00	21.45	431	0.49
22	6000	1828.8	0.96	1.56	1.73	1.39	0.39	180.21	144.79	0.47	162.50	34.15	422	0.48
21	6050	1844.0	0.60	0.81	1.10	1.11	0.42	183.33	185.00	0.42	135.00	17.73	312	0.49
20	6100	1859.3	0.78	0.89	1.29	1.55	0.40	165.38	198.72	0.41	114.10	19.48	426	
19	6150	1874.5	**1.34**	0.92	**2.34**	2.58	0.95	174.63	192.54	0.28	68.66	20.14	318	0.52
18	6200	1889.8	0.90	0.88	1.37	1.70	0.53	152.22	188.89	0.39	97.78	19.26	318	0.49
17	6250	1905.0	**1.31**	1.27	**2.22**	2.20	1.04	169.47	167.94	0.36	96.95	27.80	321	0.48
16	6300	1920.2	0.82	1.04	2.05	1.65	0.42	250.00	201.22	0.34	126.83	22.76	423	
15	6400	1950.7	0.85	0.77	1.07	1.13	0.31	125.88	132.94	0.42	90.59	16.86	295	0.51
Avg			**0.98**	**1.05**	**1.79**	**1.58**	**0.47**	**181.54**	**164.39**	**0.38**	**112.20**	**23.06**	**358.9**	
14	6450	1966.0	2.50	1.55	5.71	5.45	1.92	228.40	218.00	0.21	62.00	33.93	305	0.51
13	6500	1981.2	**7.05**	3.77	**18.27**	5.20	2.46	259.15	73.76	0.17	53.48	82.53	425	0.49
12	6600	2011.7	**4.41**	7.18	**17.17**	2.26	0.79	389.34	51.25	0.29	162.81	157.17	402	0.50
11	6650	2026.9	**4.75**	7.69	**15.14**	13.92	0.80	318.74	293.05	0.34	161.89	168.33	416	
10	6700	2042.2	**2.20**	4.82	**5.09**	1.82	0.39	231.36	82.73	0.49	219.09	105.51	422	0.49
9	6750	2057.4	**2.63**	6.04	**7.09**	2.08	0.55	269.58	79.09	0.46	229.66	132.22	420	0.49
8	6850	2087.9	0.54	0.97	1.30	0.91	0.25	240.74	168.52	0.43	179.63	21.23	411	0.50
7	6900	2103.1	**6.97**	7.70	**17.98**	9.67	4.58	257.96	138.74	0.30	110.47	168.55	312	0.52
6	6950	2118.4	**11.59**	11.48	**23.53**	4.43	1.88	203.02	38.22	0.33	99.05	251.30	415	0.52
5	7000	2133.6	**3.41**	5.34	**7.44**	1.28	0.52	218.18	37.54	0.42	156.60	116.89	424	
4	7050	2148.8	**2.49**	4.15	**4.58**	1.34	0.56	183.94	53.82	0.48	166.67	90.84	423	0.57
3	7100	2164.1	**3.15**	5.20	**5.90**	1.51	0.34	187.30	47.94	0.47	165.08	113.83	424	0.52
2	7150	2179.3	**2.16**	4.62	**4.76**	2.22	0.62	220.37	102.78	0.49	213.89	101.13	418	0.51
1	7200	2194.6	**1.14**	3.56	**2.72**	0.96	0.22	238.60	84.21	0.57	312.28	77.93	301	0.55
Avg			**3.93**	**5.29**	**9.76**	**3.78**	**1.13**	**246.19**	**104.97**	**0.39**	**163.76**	**115.81**	**394.1**	

Table 2

Samples No.	Depth ft	Depth m	TOC wt %	S1 mg HC/g rock	S2 mg HC/g rock	S3 mg CO2/g rock	S3 mg CO/g rock	HI mg HC/g TOC	OI mg HC/g TOC	PI mg HC/g rock	OSI mg HC/g TOC	Oil in Rock bbl oil/ac-ft	Tmax °C	VRo (%)
25	5850	1783.1	**1.22**	0.47	**1.66**	1.29	0.26	136.07	105.74	0.22	38.52	10.29	432	0.49
24	6000	1828.8	0.67	0.19	0.7	1.17	0.22	104.48	174.63	0.21	28.36	4.16	425	0.51
23	6050	1844.0	**1.65**	0.93	**3.25**	1.61	0.47	196.97	97.58	0.22	56.36	20.36	411	0.49
22	6100	1859.3	**1.52**	1.99	**3.81**	1.79	0.35	250.66	117.76	0.34	130.92	43.56	427	0.52
21	6150	1874.5	**2.14**	1.18	**4.7**	2.53	0.47	219.63	118.22	0.20	55.14	25.83	409	0.52
20	6200	1889.8	1.09	0.34	1.29	2.17	0.19	118.35	199.08	0.21	31.19	7.44	430	0.55
19	6300	1920.2	1.04	0.4	1.34	1.76	0.21	128.85	169.23	0.23	38.46	8.76	428	0.50
18	6350	1935.5	**1.64**	2.18	**4.8**	2.33	0.46	292.68	142.07	0.31	132.93	47.72	427	0.57
17	6400	1950.7	**1.26**	0.57	**2.28**	2.01	0.26	180.95	159.52	0.20	45.24	12.48	424	0.53
16	6450	1966.0	**1.40**	0.7	**2.14**	2.37	0.39	152.86	169.29	0.25	50.00	15.32	431	0.56
15	6550	1996.4	1.01	0.47	1.47	1.88	0.25	145.54	186.14	0.24	46.53	10.29	431	0.55
14	6600	2011.7	**1.23**	0.47	**1.49**	1.71	0.36	121.14	139.02	0.24	38.21	10.29	427	0.53
13	6650	2026.9	0.82	0.42	0.88	1	0.23	107.32	121.95	0.32	51.22	9.19	428	0.53
12	6700	2042.2	0.45	0.32	0.79	0.92	0.08	175.56	204.44	0.29	71.11	7.00	430	0.54
11	6800	2072.6	0.35	0.21	0.38	0.88	0.06	108.57	251.43	0.36	60.00	4.60	421	0.55
10	6850	2087.9	**1.33**	0.8	**2.2**	2.02	0.44	165.41	151.88	0.27	60.15	17.51	430	0.54
9	6950	2118.4	0.55	0.25	0.8	1.09	0.09	145.45	198.18	0.24	45.45	5.47	429	0.56
Avg			**1.14**	**0.69**	**1.99**	**1.67**	**0.28**	**161.79**	**159.19**	**0.26**	**57.64**	**15.31**	**425.88**	
8	7000	2133.6	1.14	0.32	1.06	2.01	0.46	92.98	176.32	0.23	28.07	7.00	428	0.58
7	7050	2148.8	1.05	0.23	1.08	2.7	0.19	102.86	257.14	0.18	21.90	5.03	425	0.52
6	7100	2164.1	1.08	0.46	1.69	1.28	0.26	156.48	118.52	0.21	42.59	10.07	429	0.55
5	7200	2194.6	0.73	0.19	0.76	2.37	0.14	104.11	324.66	0.20	26.03	4.16	429	0.56
4	7250	2209.8	0.71	0.26	0.96	1.93	0.17	135.21	271.83	0.21	36.62	5.69	431	0.55
3	7300	2225.0	0.93	0.26	1.11	1.66	0.22	119.35	178.49	0.19	27.96	5.69	428	0.56
2	7350	2240.3	0.81	0.24	1.29	1.24	0.27	159.26	153.09	0.16	29.63	5.25	430	0.55
1	7400	2255.5	0.97	0.18	1.33	1.7	0.2	137.11	175.26	0.12	18.56	3.94	432	0.59
Avg			**0.93**	**0.26**	**1.16**	**1.86**	**0.23**	**129.91**	**201.61**	**0.20**	**32.11**	**6.91**	**429**	

Table 3

Sample no.	Depth (ft)	Depth (m)	Spores	Microplankton	pollen	Rt (Sporomorphs)	Rm (Marine palynomorphs)	PMI	Spores %	Microplankton %	Pollen %
34	5600	1706.9	139	12	149.0	288.0	12	4.2	46.3	4.0	49.7
33	5650	1722.1	100	10	190.0	290	10	3.4	33.3	3.3	63.3
32	5750	1,753	126	36	138	264	36	13.6	42.0	12.0	46.0
31	5800	1,768	128	6	166	294	6	2.0	42.7	2.0	55.3
30	5850	1,783	154	11	135	289	11	3.8	51.3	3.7	45.0
29	5900	1,798	150	23	127	277	23	8.3	50.0	7.7	42.3
28	5950	1,814	212	26	62	274	26	9.5	70.7	8.7	20.7
27	6000	1,829	205	17	78	283	17	6.0	68.3	5.7	26.0
26	6050	1,844	145	30	125	270	30	11.1	48.3	10.0	41.7
25	6100	1,859	167	11	122	289	11	3.8	55.7	3.7	40.7
24	6150	1,875	0	0	0	0	0	0	0	0	0
23	6200	1,890	0	0	0	0	0	0	0	0	0
22	6250	1,905	0	0	0	0	0	0	0	0	0
21	6300	1,920	186	10	104	290	10	3.4	62.0	3.3	34.7
20	6350	1,935	171	24	105	276	24	8.7	57.0	8.0	35.0
19	6400	1,951	139	48	113	252	48	19.0	46.3	16.0	37.7
Avg						**279.7**	**20.3**		**51.8**	**6.8**	**41.4**
18	6450	1,966	227	8	65	292	8	2.7	75.7	2.7	21.7
17	6500	1,981	199	9	92	291	9	3.1	66.3	3.0	30.7
16	6550	1,996	202	7	91	293	7	2.4	67.3	2.3	30.3
15	6600	2,012	239	11	50	289	11	3.8	79.7	3.7	16.7
14	6650	2,027	211	11	78	289	11	3.8	70.3	3.7	26.0
13	6690	2,039	200	9	91	291	9	3.1	66.7	3.0	30.3
12	6750	2,057	238	5	57	295	5	1.7	79.3	1.7	19.0
11	6800	2,073	243	7	50	293	7	2.4	81.0	2.3	16.7
10	6850	2,088	0	0	0	0	0	0	0	0	0
9	6900	2,103	284	1	15	299	1	0.3	94.7	0.3	5.0
8	6950	2,118	293	0	7	300	0	0.0	97.7	0.0	2.3
7	7000	2,134	275	2	23	298	2	0.7	91.7	0.7	7.7
6	7050	2,149	269	6	25	294	6	2.0	89.7	2.0	8.3
5	7100	2,164	242	6	52	294	6	2.0	80.7	2.0	17.3
4	7150	2,179	276	2	22	298	2	0.7	92.0	0.7	7.3
3	7200	2,195	204	14	82	286	14	4.9	68.0	4.7	27.3
2	7250	2,210	209	28	63	272	28	10.3	69.7	9.3	21.0
1	7300	2,225	234	6	60	294	6	2.0	78.0	2.0	20.0
Avg						**288.8**	**7.3**		**79.3**	**2.6**	**18.1**

Table 4

Sample no.	Depth (ft)	Depth (m)	Spores	Microplankton	pollen	Rt (Sporomorphs)	Rm (Marine palynomorphs)	PMI	Spores %	Microplankton %	Pollen %
16	5850	1783.08	199	10	91	290	10	3.4	66.3	3.3	30.3
15	6050	1844.04	207	14	79	286	14	4.9	69.0	4.7	26.3
14	6200	1889.76	215	15	70	285	15	5.2	71.7	5.0	23.3
13	6300	1920.24	238	18	44	282	18	6.4	79.3	6.0	14.7
12	6400	1950.72	217	15	68	285	15	5.2	72.3	5.0	22.7
11	6500	1981.2	227	12	61	288	12	4.2	75.7	4.0	20.3
10	6550	1996.44	212	19	69	281	19	6.7	70.7	6.3	23.0
9	6650	2026.92	218	13	69	287	13	4.5	72.7	4.3	23.0
8	6850	2087.88	237	11	52	289	11	3.8	79.0	3.7	17.3
7	6900	2103.12	229	16	55	284	16	5.6	76.3	5.3	18.3
Avg			219	**14.3**	**65.**	**285.7**	**14.3**	**5.0**	**73.3**	**4.8**	**21.9**
6	7000	2133.6	243	5	52	295	5	1.7	81.0	1.7	17.3
5	7050	2148.84	236	6	58	294	6	2.0	78.7	2.0	19.3
4	7100	2164.08	201	12	87	288	12	4.2	67.0	4.0	29.0
3	7250	2209.8	195	9	96	291	9	3.1	65.0	3.0	32.0
2	7350	2240.28	210	9	81	291	9	3.1	70.0	3.0	27.0
1	7400	2255.5	171	7	122	293	7	2.4	57.0	2.3	40.7
Avg			**209.33**	**8.2**	**74.8**	**292**	**8**	**2.7**	**69.8**	**2.7**	**27.6**

Table 5

Samples No.	Depth ft	Depth m	Liptinite Group		Vitrinite (Non-opaque) Group %	Inertinite (Opaque) Group %
			(Palynomorphs) %	(AOM) %		
34	5600	1706.9	4	40.4	50.6	5
33	5650	1722.1	6	42	41	11
32	5750	1752.6	3.4	69	23.6	4
31	5800	1767.8	3.0	65.6	28.4	3.0
30	5850	1783.1	3.6	43	45.6	7.8
29	5900	1798.3	3	46.4	39.6	11
28	5950	1813.6	1	42	48	9
27	6000	1828.8	1.4	61	31.6	6
26	6050	1844.0	1.2	62.2	29	7.6
25	6100	1859.3	2	49	42	7
24	6150	1874.5	2.4	43.6	46	8
23	6200	1889.8	3.6	38	46.4	12
22	6250	1905.0	5	39	50	6
21	6300	1920.2	4	19.6	70	6.4
20	6350	1935.5	3.6	33.4	55.4	7.6
19	6400	1950.7	3.0	44.4	45.6	7.0
Avg.			**3.1**	**46.2**	**43.3**	**7.4**
18	6450	1966.0	2	66.2	25.4	6.4
17	6500	1981.2	1.8	73.2	20	5
16	6550	1996.4	2.8	43.4	47.6	6.2
15	6600	2011.7	3.6	77.2	9	10.2
14	6650	2026.9	3	80.8	7.8	8.4
13	6700	2042.2	2	84	10.4	3.6
12	6750	2057.4	2.4	87.6	7.6	2.4
11	6800	2072.6	1.6	91	5.4	2
10	6850	2087.9	1	87.6	3.8	7.6
9	6900	2103.1	2.4	62.2	33.2	2.2
8	6950	2118.4	2	70.4	26	1.6
7	7000	2133.6	2.4	68	25.2	4.4
6	7050	2148.8	4.4	62.2	27.8	5.6
5	7100	2164.1	5.8	60	31.6	2.6
4	7150	2179.3	5.4	61	29.8	3.8
3	7200	2194.6	4.4	63	27	5.6
2	7250	2209.8	6.4	60.2	25	8.4
1	7300	2225.0	5	65.2	23	6.8
Avg.			**3.2**	**70.2**	**21.4**	**5.2**

Table 6

Palynofacies field and environment		Comments	Spores: Bisaccate pollen	Microplankton	Kerogen type
II	Marginal dysoxic-anoxic basin	AOM diluted by high phytoclast input, but AOM preservation moderates to good. Amount of marine TOC dependent on basin redox state.	High	Very low	III (gas prone)
VI	Proximal suboxic-anoxic shelf.	High AOM preservation due to reducing basin conditions. Absolute phytoclast content may be moderate to high due to turbiditic input and/or general proximity to source.	Variable low to moderate	Low to common dinocysts dominant	II (oil prone)
IX	Distal suboxic-anoxic basin.	AOM-dominant assemblages. Low abundances of palynomorphs partly due to masking. Frequently alginate-rich. Deep basin or stratified shelf sea deposits, especially sediments starved basins.	Low	Generally low, prasinophyte often dominant	II ≥ I (highly oil prone)

Table 7

Samples No.	Depth ft	Depth m	Liptinite Group		Vitrinite (Non-opaque) Group %	Inertinite (Opaque) Group %
			(Palynomorphs) %	(AOM) %		
16	5850	1783.08	3.60	22.6	72.20	1.60
15	6050	1844.04	4	30.4	63.2	2.4
14	6200	1889.76	3.8	20	72.6	3.6
13	6300	1920.24	3	21	70.6	5.4
12	6400	1950.72	5	27	64.4	3.6
11	6500	1981.2	4	24.6	69.4	2
10	6550	1996.44	3.6	19.4	73.6	3.4
9	6650	2026.92	2	18.2	75.4	4.4
8	6850	2087.88	3	34	60	3
7	6900	2103.12	3	39.4	56	1.6
Avg.			**3.50**	**25.7**	**67.7**	**3.16**
6	7000	2133.6	3	33	63	1
5	7050	2148.84	2.8	38.6	56	2.6
4	7100	2164.08	1	43	54.6	1.4
3	7250	2209.8	4.6	34	59.6	1.8
2	7350	2240.28	4	35.6	58.6	1.8
1	7400	2255.5	5	32	62	1
Avg.			**3.4**	**36**	**58.9**	**1.6**

Table 8

Sample no.	Depth (ft)	Depth (m)	Dinocyst %	MFTLs %	Pteridophyte spores %	Freshwater Algae %	Spherical pollen grains %	PMI	Non-opaque wood %	Opaque wood %	AOM %
16	5850	1783.08	2.7	0.7	59.0	0.0	26.3	3.4	72.20	1.60	22.6
15	6050	1844.04	2.7	2.0	62.3	0.0	16.3	4.9	63.2	2.4	30.4
14	6200	1889.76	4.3	0.7	64.7	0.0	14.3	5.2	72.6	3.6	20
13	6300	1920.24	3.7	2.3	66.7	0.0	11.0	6.4	70.6	5.4	21
12	6400	1950.72	3.0	2.0	68.0	0.0	17.7	5.2	64.4	3.6	27
11	6500	1981.2	3.0	1.0	70.0	0.0	16.7	4.2	69.4	2	24.6
10	6550	1996.44	5.3	1.0	67.7	0.3	20.3	6.7	73.6	3.4	19.4
9	6650	2026.92	3.7	0.7	66.7	0.0	19.3	4.5	75.4	4.4	18.2
8	6850	2087.88	2.7	1.0	69.3	0.0	16.0	3.8	60	3	34
7	6900	2103.12	4.0	1.3	67.0	0.0	15.0	5.6	56	1.6	39.4
Avg			**3.5**	**1.3**	**66.1**	**0.03**	**17.3**	**5.0**	**67.7**	**3.1**	**25.7**
6	7000	2133.6	1.7	0.0	74.0	0.0	14.3	1.7	63	1	33
5	7050	2148.84	2.0	0.0	71.0	0.0	16.0	2.0	56	2.6	38.6
4	7100	2164.08	3.3	0.7	58.3	0.0	10.0	4.2	54.6	1.4	43
3	7250	2209.8	1.7	0.7	56.7	0.0	24.7	3.1	59.6	1.8	34
2	7350	2240.28	3.0	0.0	63.3	0.0	18.3	3.1	58.6	1.8	35.6
1	7400	2255.5	1.3	1.0	52.0	1.0	31.7	2.4	62	1	32
Avg			**2.2**	**0.4**	**62.6**	**0.2**	**26.3**	**2.7**	**58.9**	**1.6**	**36**